Published in final edited form as:
J Mol Biol. 2008 September 19; 381(5): 1114–1132. doi:10.1016/j.jmb.2008.04.034.

DNA Packaging Motor Assembly Intermediate of Bacteriophage φ29

Jaya S. Koti[1,5], **Marc C. Morais**[3,†], **Raj Rajagopal**[1], **Barbara A. L. Owen**[4], **Cynthia T. McMurray**[4], and **Dwight L. Anderson**[1,2,*]

1*Department of Diagnostic/Biological Sciences, University of Minnesota, Minneapolis, MN 55455, USA*

2*Department of Microbiology, University of Minnesota, Minneapolis, MN 55455, USA*

3*Department of Biological Sciences, Purdue University, West Lafayette, IN 47907, USA*

4*Departments of Biochemistry and Molecular Biology, Department of Medical Pharmacology and Experimental Therapeutics, Mayo College of Medicine, Rochester, MN 55905, USA.*

Abstract

Unraveling the structure and assembly of the DNA packaging ATPases of the tailed, double-stranded DNA bacteriophages is integral to understanding the mechanism of DNA translocation. Here the bacteriophage ϕ29 packaging ATPase, gene product gp16 (gp16), was over-expressed in soluble form in *Bacillus subtilis* (pSAC), purified to near homogeneity, and assembled to the ϕ29 precursor capsid (prohead) to produce a packaging motor intermediate that was fully active in *in vitro* DNA packaging. The formation of higher oligomers of the gp16 from monomers was concentration dependent and was characterized by analytical ultracentrifugation, gel filtration and electron microscopy. The binding of multiple copies of gp16 to the prohead was dependent upon the presence of an oligomer of 174- or 120-base prohead RNA (pRNA) fixed to the head-tail connector at the unique portal vertex of the prohead. The use of mutant pRNAs demonstrated that gp16 bound specifically to the A-helix of pRNA, and ribonuclease footprinting of gp16 on pRNA showed that gp16 protected the CC residues of the CCA bulge (residues 18–20) of the A-helix. The binding of gp16 to the prohead/pRNA to constitute the complete and active packaging motor was confirmed by cryo-electron microscopy three-dimensional reconstruction of the prohead/pRNA/gp16 complex. The complex was capable of supercoiling DNA-gp3 as observed previously for gp16 alone, and therefore the binding of gp16 to the prohead, rather than first to DNA-gp3, represents an alternative packaging motor assembly pathway.

Keywords

DNA packaging; ATPase gp16; phage assembly; bacteriophage ϕ29; RNA binding

*Corresponding author: Telephone, 612-624-7989; Fax, 612-626-1108; E-mail, dlander@umn.edu.
[5]Current address: Instrument Systems Development Center, Beckman Coulter Inc., Chaska, MN 55318, USA.
[†]Current address: Department of Biochemistry and Molecular Biology, University of Texas Medical Branch, Galveston, TX 77555, USA

Introduction

The packaging of the genomes of the tailed, double-stranded DNA (dsDNA) bacteriophages into preformed protein capsids (proheads) is a remarkable process in which the highly charged DNA is compacted to near crystalline density.[1, 2] Molecular motors assembled at the unique portal vertex of the prohead drive packaging, converting energy obtained from ATP hydrolysis to power DNA translocation. The motor in bacteriophage ϕ29 is among the most powerful biological motors known, generating forces in the range of 60–100 picoNewtons.[3, 4] The packaging machines include a ring of ATPases (terminases), the head-tail connector of the prohead, the prohead and the DNA substrate. These components show many biochemical and structural similarities, suggesting a common mechanism for DNA translocation.[5–7] Terminases belong to a large family of ATPases involved in DNA transactions such as cell division, chromosome segregation, recombination, strand separation, and conjugation.[8, 9] Each terminase has large and small subunits: the large subunit has prohead and ATP binding activities, potential magnesium binding motifs and endonuclease activity.[9–14] The terminase small subunit has DNA binding and packaging stimulation activities. Unraveling the structure, assembly and function of packaging ATPases is essential in gaining an understanding of the packaging mechanism.

In the DNA packaging system of the *Bacillus subtilis* bacteriophage ϕ29, gene product 16 (gp16) corresponds to the large terminase subunit, and gp3 terminally bound to the 5' DNA ends (DNA-gp3) represents the small subunit.[15] *In vitro* and *in vivo* encapsidation of ϕ29 DNA-gp3 into proheads requires gp16,[16, 17] a 39 kDa protein with the Walker A and Walker B motifs needed for ATP hydrolysis. Although ϕ29 is one of the best-characterized systems for study of the dsDNA packaging mechanism, and the structure of the head-tail connector is determined,[18, 19] limited structural information is available for gp16 and its assembly to constitute the packaging motor. Detailed physical and biological characterization of gp16 has been challenged by its insolubility after over-expression and purification. Expression of gp16 in *E.coli* yielded inclusion bodies, and because the bulk of the protein was insoluble after renaturation, about 100 copies of protein were needed to package each ϕ29 DNA in the completely defined *in vitro* system.[20]

The unique features of ϕ29 DNA-gp3 packaging are i) the DNA-gp3 packaging substrate is supercoiled by the concerted action of gp16 and gp3 in the absence of the prohead, and the preferential packaging of this DNA/gp3/gp16 complex suggests that gp16 constitutes the packaging motor while bound to DNA;[21] ii) a 174-base ϕ29-encoded RNA (or its 120-base derivative) (prohead RNA, pRNA) is an essential packaging motor component;[22] iii) pRNA binds to the connector of the prohead,[23] and cryoEM reconstructions show that gp16 binds to the pRNA[18] iv) the ATPase activity of gp16 is pRNA-dependent,[24] such that the ATPase "subunits" of the packaging motor may be gp16-pRNA heterodimers; and v) *in vitro* packaging rivals *in vivo* packaging in efficiency,[2, 16, 20] facilitating study of the packaging mechanism.

pRNA binds to the prohead in a specific, rapid, irreversible, and magnesium-dependent reaction.[25–31] Although pRNA and gp16 are essential to DNA packaging, their presence is transitory during phage assembly, as both components are displaced during neck/tail assembly and are absent in the mature phage.[32] Two functional regions of pRNA, a prohead binding region and a region involved in DNA translocation, have been identified.[33–36] Bases 22–84 of the pRNA were identified to be the prohead binding domain by ribonuclease footprinting, and this was confirmed by mutant studies and competitive binding experiments.[26, 33, 34] While the prohead binding domain is well characterized, knowledge of the gp16-binding domain has been rudimentary.

A mechanistic understanding of the DNA packaging process in ϕ29 and other dsDNA phages is lacking in spite of extensive biochemical, structural, biophysical and theoretical studies.[2, 14] A model for how ϕ29 DNA is translocated into the capsid was proposed in which ATP binding, hydrolysis, and release of products induce conformational changes in the ATPases that are directly involved in the translocation of the DNA.[37] DNA translocation is triggered by or performed by the ring of ATPases, possibly in concert with other motor components such as the head-tail connector, via a conformational change that likely follows release of phosphate after ATP hydrolysis.[37] Many of the packaging mechanism models have been based on rotation of the head-tail connector.[2, 38] However, recent evidence suggested that the T4 connector does not rotate during DNA translocation,[39] and a direct test by following the orientation of single fluorophores attached to the connector provided evidence that the ϕ29 connector does not rotate.[40] In phage SPP1, amino acid loops in the connector channel that tightly embrace DNA are proposed to form an undulating 'wave' of conformational change as DNA is translocated, which may coordinate ATP hydrolysis whether force is applied by the ATPase itself or by ATPase-induced conformational change in the connector.[41] On the basis of a crystal structure of the ATPase gp17 of phage T4 at 1.8Å and the similarity of this structure to monomeric helicases, it was proposed that DNA is translocated by the gp17 itself, with each monomer in the ring of ATPases sequentially detecting the same DNA structural component after translocation of DNA by two base pairs.[9]

Here, over-expression of gp16 in its natural *Bacillus subtilis* host is described. The protein has been purified to greater than 99% homogeneity to obtain soluble and highly active protein in milligram quantities needed for structural and functional studies. The physical state of the protein in solution is described as well as its pRNA- and DNA-binding properties. An alternative pathway of gp16 assembly to the prohead prior to interaction with DNA-gp3 is documented. Multiple copies of gp16 interact with the prohead-bound pRNA oligomer to constitute the DNA packaging motor, and the isolated prohead/pRNA/gp16 complex is active in DNA packaging without the aid of additional gp16. The pRNA-gp16 interaction is ATP independent, and the gp16 binding is shown to be A-helix specific by the use of pRNA mutants and RNase footprinting. Cryo-EM reconstruction demonstrates that the pRNA-gp16 oligomers are both five-fold symmetric and interfaced such that the motor subunits may be gp16-pRNA heterodimers.

Results

Production of soluble gp16, purification, and biological activity

Production of gp16 in *E. coli* (pPLc2833) yields inclusion bodies, and the bulk of the highly hydrophobic protein is insoluble after treatment of isolated inclusion bodies with guanidinium chloride, followed by urea,[20] making detailed physical and biological characterization of this DNA packaging ATPase impossible. To circumvent this, gene 16 was expressed in *B. subtilis*, yielding soluble gp16 that has long been the source of ATPase for packaging assays.[21] However, the details of plasmid construction and the purification of milligram amounts of protein to near homogeneity have not been published. Briefly, the *Eco*RI E/D segment of ϕ29 DNA-gp3 that includes gene 16,[42] obtained by partial digestion, was cloned into the plasmid pUB18. The sucrose inducible promoter SACB[43] was inserted to drive expression, and the resulting plasmid pSACB-gp16 was transformed into *B. subtilis* WB30, an asporogenic, protease-defective strain. After induction of gene 16 expression with sucrose (Methods), about 70% of the gp16 was soluble. The 39 kDa gp16 was purified to near homogeneity by cation exchange followed by hydroxyapatite chromatography (Figure 1(a)). The pI of the purified protein was estimated at 10.2 by isoelectrofocussing, and its identity was confirmed by Western blotting with polyclonal anti-gp16 serum.

The activity of purified gp16 in *in vitro* DNA-gp3 packaging was determined by a standard DNase protection assay (Figure. 1(b)).[44] Purified gp16 was highly active, and multiple copies were required per prohead for DNA-gp3 packaging (Figure 1(b)). No DNA-gp3 packaging was detected in the absence of ATP or gp16 (Figure 1(b) lanes 2 and 10). A 4-fold reduction in gp16 resulted in a 40-fold reduction in packaging. These results are consistent with the *in vitro* DNA-gp3 packaging in extracts, which shows a first order concentration dependence for the prohead and DNA-gp3, while multiple copies of the packaging ATPase gp16 are required.[45]

Monomeric/multimeric state of gp16

No large aggregates of the purified gp16 at concentrations of 0.8 mg/ml were detected by dynamic light scattering, and the hydrodynamic radius of 6 to 9 nm (data not shown) suggested that the protein was soluble and formed an oligomer. To determine the oligomeric state of gp16, sedimentation equilibrium centrifugation was performed. The calculated monomer molecular weight of gp16 based on the amino acid sequence is ~39 kDa. Sedimentation equilibrium centrifugation confirmed that gp16 self-associates, giving molecular weights greater than monomer and an apparent molecular mass that varied with the protein concentration (Table 1). The apparent molecular mass of gp16 at various concentrations and speeds was derived by fitting the data to a self-association model using NONLIN.[46] Figure 2 (a) shows the A280 versus $r^2/2$ plots for gp16 at three protein concentrations at 11,000 rpm. 80–85% of the protein was a trimer and the remainder was a monomer as determined by species analysis using the sedimentation analysis software, SEDPHAT.[47] A trimer of gp16 would have a molecular weight of ~117 kDa, and this is the most abundant species at 0.2 mg/ml or at 11,000 rpm (Table1). However, fits of the data consistent with only monomer to trimer models were unsatisfactory, indicating that additional species may be present. Furthermore, the data at higher protein concentrations and lower centrifugation speeds suggested that species larger than trimer were present. SEDPHAT[47] was used to determine the relative concentrations of additional species. Figure 2(b) shows a plot of A280 versus the radial position at 0.4 mg/ml and at 8,000 rpm. The data was fit with four possible species, monomer, trimer, hexamer and dodecamer. The best fit of the data yielded 22, 68 and 10% of monomer, trimer and dodecamer, respectively. The relatively small and random distribution of the residuals attests to the goodness of this fit. Indeed, other models tried, such as monomer, dimer, tetramer, yielded poor fits to the data. A kd for the oligomerization could not be obtained because gp16 was relatively difficult to maintain in a soluble state. At protein concentrations of 0.2–0.4 mg/ml, approximately 40% of the total protein was irreversibly lost even at speeds as low as 5,000 rpm. This loss increased to 65% at 0.8 mg/ml, but additional loss was not seen at the higher centrifugation speeds of 8,000 and 11,000 rpm. Non-reducing PAGE was done after the centrifugation to look for degradation and oxidized cysteine-driven oligomerization, and no protein degradation was detected.

Secondary plots of the sedimentation equilibrium primary data (data not shown) indicated that gp16 was monomeric at protein concentrations below 100 μg/ml. To confirm these findings, gel filtration chromatography was performed at gp16 concentrations between 10 and 100 μg/ml. Buffer and temperature conditions were exactly the same as those used in the sedimentation equilibrium experiments. Figure 2(c) shows the elution profile of 100 μg/ml gp16 on a superdex-200 column (dashed line) with molecular weight markers (solid line). gp16 eluted slightly ahead of a protein standard having a molecular weight of 44,000, consistent with gp16 being monomeric at concentrations less than 100 μg/ml as suggested by the analytical ultracentrifugation results.

Transmission electron microscopy of the purified gp16 at 50 ug/ml was done to determine the size and shape of gp16. Figure 2 (d) and (e) show purified gp16 negatively stained with uranyl

acetate. gp16 appeared as rounded and porous oligomers with a diameter of 9.5 +/− 1.5 nm, calculated from the area. Figure 2 (f) shows a histogram of the multimer diameter measurements. Monomers likely were not visualized because of small size, and it is not known to what extent increase in protein concentration during drying of the specimen contributed to formation of the multimers. Variation of the pH, salt conditions, staining methods or the presence of ATP did not alter the structure of gp16 by TEM.

Characterization of the gp16-pRNA interaction

Interaction between the ATPase gp16 and prohead RNA (pRNA) has been documented by the stimulation of the ATPase activity of gp16 by prohead-bound pRNA, which is needed continuously for ATP hydrolysis;[24] the presence of additional mass on the pRNA spokes of partially packaged particles in a cryo-EM 3D reconstruction, interpreted as gp16;[18] the binding of pRNA to gp16 on nitrocellulose filters;[48] the weak binding of pRNA to thioredoxin HIS-tag gp16 fusion protein immobilized on a HIS-bind column;[49] and recent delineation of the molecular boundaries of the components of the packaging motor by cryoEM reconstruction (Morais et al., submitted).

To characterize the gp16-pRNA interaction in solution, 120-base pRNA was incubated with increasing concentrations of gp16 and the interaction assessed by electrophoretic mobility shift assay (EMSA) in a native agarose gel (Figure 3(a)). Mixed 1:1 (based on monomers), much of the pRNA disappears from its fast migration position (compare lanes 1 and 2), suggesting that the pRNA and gp16 interact to produce heterogeneous complexes that do not appear in the gel. Three copies of gp16 per pRNA (lane 3) were sufficient to shift the pRNA band in the gel, and as the copy number of gp16 per pRNA was increased, more of the pRNA/gp16 complex was retained in the wells of the gel. gp16 bound to 174-base pRNA in the same manner (data not shown). The pRNA-gp16 interaction was independent of ATP. The complex was stable in the presence of 100 mM EDTA and overnight incubation at 4°C but was disrupted by 0.1% SDS. pRNA-gp16(1:3) complexes were mixed and incubated with fiberless proheads (10:1), and following isolation by electrophoresis on a native agarose gel, the particles were tested for pRNA binding by staining with ethidium bromide and for gp16 binding following transfer to nitrocellulose and development with anti-gp16 serum. Both pRNA and gp16 were found on the prohead, and excess pRNA/gp16 migrated as a complex (data not shown).

pRNA can be removed from the ϕ29 prohead by treatment with EDTA or with RNase A, resulting in loss of DNA packaging activity, and reconstitution of these pRNA-free proheads with purified pRNA results in restoration of packaging activity in the defined *in vitro* system.[22,50] pRNA-free proheads were reconstituted with 120-base pRNA/gp16 (1:3) complexes and the particles tested in the *in vitro* DNA-gp3 packaging system.[44] The efficiency of packaging was dependent on the number of pRNA/gp16 complexes (mixed as 1 pRNA: 3 gp16) per prohead (Figure 3(b)). Proheads were 2-fold in excess over DNA-gp3, and all of the DNA-gp3 was packaged when 5–7 copies of pRNA and its associated gp16 were used per prohead in the *in vitro* DNA-gp3 packaging reaction. As pRNA is pentameric in cryoEM reconstruction[30] (Figure 7(d)), the results suggested that nearly every pRNA molecule added was biologically active and that the gp16 molecules were also highly active.

Isolation of a prohead/gp16 ATPase motor assembly intermediate

Prior evidence for prohead-gp16 interaction was obtained by sucrose density gradient centrifugation and ELISA tests,[15, 48] but the role of pRNA in the interaction was not clear. To determine the role of pRNA in the prohead-gp16 interaction, sucrose density gradient centrifugation was used. Figure 4 shows the predicted secondary structures of the various forms of pRNA tested for gp16 binding. Proheads with 174-base pRNA[51] (see following paragraph) were incubated with 20 copies of gp16 per prohead and the complexes sedimented in a sucrose

density gradient (Figure 5(a)). There was a clear shift in the position of proheads incubated with gp16, and the fast-sedimenting particles were isolated and shown by SDS-PAGE to contain gp16 (Figure 6(a), lane 2). The copies of gp16 per prohead from densitometric analysis was about one-half of that of the head-tail connector, which is known to contain 12 copies of gp10.[18] This prohead/174-base pRNA/gp16 interaction is Mg^{2+} dependent and ATP independent. Proheads and gp16 interacted at high ionic strength (100 mM NaCl), but low ionic strength (10 mM) was needed to retain the bound gp16. The prohead/174-base pRNA/gp16 complexes isolated from the sucrose gradient were tested for *in vitro* DNA-gp3 packaging activity upon addition of DNA-gp3 and ATP (Figure 6(b)). The isolated prohead/174-pRNA/ATPase intermediate packaged DNA-gp3 without further addition of gp16 (lane 5), and with the same efficiency as proheads with 174-base pRNA mixed with gp16 in the *in vitro* reaction (lane 3), as the concentration of proheads used in the reaction of lane 3 was ~2-fold higher than that represented in lane 5. Figure 6(b), lane 7 shows that packaging remained about the same upon addition of more gp16, and thus the isolated prohead/174-base pRNA/gp16 complex is a true intermediate with an intact and active packaging motor. The intermediate is stable and active in packaging after overnight storage at 4°C. Also, just as EDTA treatment releases pRNA from the prohead,[22] EDTA releases pRNA-gp16 as a complex from the prohead (data not shown).

174-base pRNA (with domains I and II)[51] is cleaved to a 120-base form (domain I) by adventitious ribonucleases during prohead isolation, and both forms are active in reconstituting pRNA-free proheads for DNA-gp3 packaging.[25] RNA-free proheads were reconstituted with 120-base pRNA (Figure 4(a)), purified by sucrose density gradient centrifugation, incubated with gp16 and run again on a sucrose gradient to determine the role of the 54-base domain II in the prohead-gp16 interaction. gp16 co-sediments with proheads containing 120-base pRNA just as with proheads having 174-base pRNA, and the isolated prohead/120-base pRNA/gp16 complex is functional in DNA-gp3 packaging (data not shown). Thus domain II of pRNA was confirmed to be dispensable for *in vitro* packaging as shown previously.[25] Figure 6(c), lane 2 shows the composition of the prohead/120-base pRNA/gp16 complexes on a native agarose gel. A Western blot of the particle developed with anti-gp16 serum confirmed the presence of gp16 on these proheads (data not shown).

pRNA dependency of the prohead-gp16 interaction and identification of the gp16 binding site on pRNA

The prohead-gp16 interaction is pRNA dependent, as pRNA-free proheads incubated with gp16 did not show the characteristic faster sedimentation demonstrated for the prohead/pRNA/gp16 particles on a sucrose gradient (Figure 5 (b)), and gp16 was not found on the isolated particles by SDS-PAGE (data not shown). Thus, stable binding of gp16 to proheads required pRNA.

Two functional domains of pRNA have been identified, a prohead binding domain and a segment involved in DNA translocation.[33–35] The prohead binding domain consists of bases 22–84 and was identified by ribonuclease footprinting and competitive binding experiments, while the A-helix that contains bases 1–28 and 117-92 was predicted to interact with gp16 (Figure 4(a)).[18] To further define the gp16 binding site on the A helix, mutant pRNAs with truncations of the A-helix were employed (Figure 4(b)–(d)). 71-base pRNA is an A-helix deletion mutant, which retains the prohead binding activity of 120-base pRNA but cannot support *in vitro* DNA-gp3 packaging.[34] pRNA-free proheads reconstituted with 71-base pRNA and purified were incubated with gp16 and the mixture sedimented in a sucrose density gradient (Figure 5(c)). The sedimentation profiles of particles reconstituted with 71-base pRNA, without and with gp16 incubation, were similar, and no gp16 was detected on particles

by SDS-PAGE. These results confirm that the prohead-gp16 interaction is mediated by pRNA and show directly that the A-helix is the site of gp16 binding.

To further define the sequences and elements of the pRNA A-helix needed for gp16 binding, pRNA-free proheads were reconstituted with two different pRNA deletion mutants and studied for gp16 binding by use of sucrose gradient centrifugation and SDS-PAGE of the isolated particles. Mutants lacking the CCA bulge at positions 18–20 of pRNA (R7 mutant, Figure 4(d)), or the 14 residues at the 3′end of the A-helix (106-base pRNA, Figure 4(b)) have prohead binding competitor activity but no DNA-gp3 packaging activity.[33] pRNA-free proheads reconstituted with these mutant pRNAs were able to bind gp16, indicating that the CCA bulge or the 14 bases at the 3′end of the A-helix were not required for the initial gp16-pRNA interaction, although particles so constituted were not active in DNA packaging (Table 2).

RNase footprinting of gp16 on pRNA

To define the nucleotides of pRNA protected by gp16, ribonuclease footprinting analysis of 5′ end-labeled [^{32}P]120-base pRNA was performed with the RNases A, T1 and V1. Proheads reconstituted with [^{32}P]120-base pRNA were separated from unbound labeled pRNA by centrifugation and used to produce footprints. In addition, free [^{32}P]120-base pRNA was also complexed with gp16 for mapping of the gp16 interactive domain. Both free pRNA and prohead-bound pRNA complexed with gp16 were protected from RNase A digestion at residues 8 to 19, 5′ to 3 ′(Figure 7(a), (b)). RNase T1 did not produce cleavage outside the prohead binding domain and was not useful for the current studies. Footprints produced with RNase V1 showed additional protection at residues 5 and 31 (data not shown). The present results confirmed the ribonuclease footprint of the prohead on pRNA, which demonstrated protection of residues 22–84 by the prohead with RNase V1 and enhanced cleavage of pRNA at residues 38–40 (data not shown)[26].

Cryo-EM 3D-reconstruction of the prohead/pRNA/ gp16 packaging intermediate

The electron dense pRNA-spokes that radiate from the head-tail connector in cryo-EM reconstructions were postulated to be A-helices.[18] A cryo-EM reconstruction of pRNA-free proheads reconstituted with 71-base pRNA lacking the A-helix has confirmed this hypothesis (Morais et al., submitted). Cryo-EM 3D reconstruction of the prohead/174-base pRNA/gp16 motor assembly intermediate showed mass that bridged the pRNA spokes and was interpreted as gp16 (Figure 7(d)–(g)). The localization of gp16 on the A-helix of pRNA was consistent with the sucrose density gradient sedimentation (Figure 5) and ribonuclease footprinting (Figure 7(a)–(b)) results.

The presence of gp16 on the DNA-filled head was also demonstrated by incubating proheads/pRNA for 10 min (too short a time for tail assembly) in an extract of cells from a restrictive infection with the ϕ29 mutant *sus*7(614)-*sus*8(769)-*sus*14(1241), which is defective for the prohead scaffolding and major capsid proteins but that served as a source of DNA-gp3 and excess gp16. The filled heads were isolated on a sucrose density gradient and analyzed by SDS-PAGE (Figure 8) and Western blotting (data not shown). gp16 remains on the filled head, apparently until displaced by subsequent neck/tail assembly. These results are consistent with the presence of gp16 on filled heads produced by *in vitro* complementation of extracts providing proheads and gp16.[17] Also, DNA-gp3 packaged into purified proheads in the defined *in vitro* system yielded filled heads containing gp16 following sucrose gradient purification (data not shown).

Binding and supercoiling of DNA-gp3 by the prohead/pRNA/gp16 motor assembly intermediate

gp16 binds and supercoils DNA-gp3 *in vitro*, and each coiled DNA retains about 3 copies of gp16 when isolated in a sucrose density gradient.[21] This interaction of gp16 with DNA-gp3 is independent of the prohead, and the DNA-gp3/gp16 complex is packaged preferentially. To reconcile these results with the present demonstration of the prohead/pRNA/gp16 intermediate and to gain insight on the order of assembly of gp16 in the initiation of DNA packaging *in vitro*, the DNA-gp3 sedimentation assay was performed as described.[21] [^{3}H]DNA-gp3 sedimented in the sucrose gradient as a peak centering on fraction 16 (Figure 9(a), black line). When DNA-gp3 was preincubated with gp16, the sedimentation rate of more than one-half of the molecules increased to give a new peak at fraction 13 (Figure 9(a), pink line). A Western dot-blot of the sucrose gradient fractions, developed with anti-gp16 serum, confirmed the co-sedimentation of gp16 with DNA-gp3 (Figure 9(c)) [Figure 9(b) shows the position of gp16 alone in the gradient]. Addition of proheads/pRNA did not alter the sedimentation state of DNA-gp3 (Figure 9(d), green line). The prohead/pRNA/gp16 intermediate (Figure 9(d)), yellow line) produced a faster-sedimenting DNA-gp3, just as did gp16 (Figure 9(d), pink line). The presence of proheads and gp16 on the fast sedimenting DNA-gp3 was confirmed by Western blotting with anti-gp10 and anti-gp16 sera, respectively. These results suggested that gp16, assembled as a component of the DNA packaging motor onto proheads/pRNA, was able to bind and supercoil the DNA-gp3 to produce an initiation complex for DNA packaging. While this interaction and formation of the higher order complex is gp3-dependent, EMSA showed that gp16 binds non-specifically to all *Hpa*I fragments of proteinase K-treated DNA-gp3 (Figure 9(e)).

Discussion

The ATPase gp16 is a central component in packaging of the ϕ29 genome, interacting with pRNA and DNA-gp3 to constitute the packaging motor at the capsid portal vertex and then providing the energy for DNA translocation. The ATPase (terminase) large subunits of the dsDNA phages and Herpesvirus tend to be insoluble,[1, 52] and production of the highly hydrophobic gp16 in soluble form for study of structure and function has been problematic. Inclusion bodies of gp16 produced in *E. coli* (pPLc 2833) could only be partially solubilized by the use of guanidinium chloride followed by urea, and therefore about 100 molecules were used to package each DNA-gp3 *in vitro*.[20] Co-expression of gp16 with GROESL in *E. coli* with the intent of producing soluble protein resulted in an excess of GROESL which had to be removed.[48] The production of gp16 with an N-terminal thioredoxin and His-Tag in *E. coli* resulted in insoluble and inactive protein.[53] Treatment with acetone or PEG was needed to improve the solubility of the gp16-His-thioredoxin, and the protein was inactive in the acetone/PEG after the thioredoxin was cleaved away, making structural or functional studies of the native protein impossible. The present preparation of gp16 in highly purified and soluble form in *Bacillus subtilis* (pSAC) will facilitate studies of gp16 structure and function.

The number of copies of the large terminase ATPase subunit required for optimal packaging activity is not fully understood, although in T3 biochemical data suggests that 6 copies are needed,[11] and in T4, gp17 is predicted to form a ring surrounding the DNA on the procapsid.[54] All the known terminase large subunits with ATPase activity exist predominantly as monomers in solution.[55–59] Self-association of terminase monomers into oligomers has been reported by sedimentation velocity in λ and by chemical crosslinking in T4 phage.[13,14] gp16 exists in solution predominantly in a monomeric state at concentrations of 0.1 mg/ml, with trimers and higher order structures at concentrations of 0.2–0.8 mg/ml as seen by gel filtration, sedimentation equilibrium studies, and electron microscopy (Figure 2). Early *in vitro* packaging studies demonstrated higher order concentration dependence for gp16, showing that

multiple copies of gp16 were needed, while concentration dependence for proheads and DNA-gp3 was first order.[16] The present study of gp16 produced in *Bacillus subtilis* (pSAC) shows that the quantity of gp16 that was found on the isolated, fully active prohead/pRNA/gp16 complex by SDS-PAGE was about one-half that of the dodecameric connector (Figure 6(a)). Similarly, terminase large subunits of phages T3, T7 and P22 bind the procapsid.[60–62] In phage λ, packaging is initiated by docking of the DNA-terminase (complex I) at the portal vertex, and amino acids of the large subunit C terminus are responsible for the capsid binding.[63, 64]

Amino acid sequence analysis indicates that the N-termini of many terminase large subunits have a conserved ATPase center.[8] All known and predicted members of DNA packaging ATPase large subunits belong to the P-loop NTPase fold which have conserved nucleotide binding (Walker A) and Mg^{+2} binding motifs (Walker B).[8, 15] The ATPase domains of T4 gp17 and ϕ29 gp16 appear to be similar. For example, the Walker B mutant D118E/E119D in gp16 of ϕ29 is inactive in DNA packaging (data not shown) as is the mutant D255E/E256D in T4 gp17, which binds ATP but is unable to precisely orient the ATP molecule.[9] Also, the crystal structures of P4 of ϕ12 and gp17 of T4 show a common ATPase domain.[9,65] However, comparative genomic studies indicate that gp16 of ϕ29 may be a diverging independent lineage from the HerA/FtsK ATPases.[66, 67] Sequence alignment and mutation data suggest that the adenine-binding motif[54] is not conserved among the gp16 analogs and is different from that of T4 gp17 (data not shown). Massey *et al.*[68] have shown that FtsK ATPase exists as a monomer in solution, and formation of hexameric rings around DNA was dependent only on the presence of DNA and was independent of nucleotide or magnesium ions. The FtsK ATPase, like gp16, differs from terminases in lacking domain fusions with their nuclease partners.

The ϕ29 DNA packaging motor differs primarily from its counterparts among the dsDNA phages by having an essential RNA component, pRNA. To date, pRNA has been confirmed only in ϕ29 and its relatives,[51] although Acidianus bottle shaped virus (ABV), an archaeal phage, produces RNA with a predicted secondary structure similar to pRNA.[69] Binding of pRNA to the head-tail connector requires the basic residues RKR at the gp10 N terminus[23] and is the last step in morphogenesis of the mature prohead. Then gp16 binds to the pRNA oligomer to constitute the active packaging motor, and this binding was strictly dependent upon and mediated by the presence of pRNA (Figure 5 and Figure 6). Ribonuclease footprints of gp16 on the prohead/pRNA showed protection of residues of the A-helix, extending to residues 18–19 which correspond to CC of the CCA bulge (Figure 7). This result was confirmed by demonstration that mutant pRNA lacking the A-helix did not bind gp16 (Figure 5(c)) and by cryo-EM reconstruction of the prohead-gp16 motor assembly intermediate which showed that gp16 was bound to the A-helix spokes of pRNA (Figure 7). The 120-base pRNA ΔCCA bulge mutant has prohead binding competitor activity but no DNA-gp3 packaging activity.[33] Even though the CC residues in the pRNA CCA bulge contribute to the gp16 binding, they were not required for the initial pRNA-gp16 interaction (Figure 4). This is similar to a previous report that the CCA bulge is dispensable for gp16 binding.[49] The His-gp16-thioredoxin was found to bind DNA nonspecifically and also to bind the pRNA/prohead more strongly than the pRNA-free capsid, although none of these complexes were tested for DNA packaging activity.[49] The RNase footprinting of gp16 on the prohead (Figure 7) should help model the gp16-pRNA interaction. Endonuclease activity possessed by other phage large terminase subunits is not needed in ϕ29 as the DNA is unit length and not packaged from a DNA concatemer.

In cryoEM reconstruction the pRNA and gp16 subunits have five-fold symmetry and are intimately associated (Figure 7). This and the fact that gp16 is a pRNA-dependent ATPase[24] lend credence to the idea that the ATPase subunits of the motor may be gp16/pRNA heterodimers. Once the gp16 has bound to pRNA, the pRNA subunits have been shown by cryoEM reconstruction to make contacts with the capsid, which rationalizes the finding that

the ring of motor subunits is five-fold symmetric.[30] Thus, pRNA ultimately links the gp16 to the capsid, and whether and how tightly pRNA remains associated with the connector is unknown. The connector is shown by cryoEM reconstruction to be essentially situated in a basket formed by pRNA.[30] In conflict with the above scenario, Ibarra *et al.*,[48] reported that, by the use of ELISA and immuno-precipitation experiments, the connector N-terminus can bind gp16, as V8-treated connectors that lack the N-terminus did not interact with gp16; pRNA-gp16 interaction was also reported in this study. The gp16 used was in high excess in these experiments (3137/prohead, 115/connector and 3.3×10^4/RNA), and none of these complexes were shown to be active in DNA packaging.

It is not known if the pRNA molecules retain their novel intermolecular base pairing interactions[70, 71] in the active packaging motor, which might serve as a means of communication among the ATPases in the coordination of motor function. The pRNA subunits have been hypothesized to function sequentially, as incorporation of one inactive subunit of a mutant pRNA has been reported to be sufficient to stop DNA packaging.[27, 72] Tests of the sequential mode of action of gp16 (and the proposed pRNA/gp16 heterodimers) are an aim of single molecule packaging studies in process.

ϕ29 gp3, covalently bound at the DNA 5' termini (DNA-gp3), is needed for DNA packaging and has been viewed as a small terminase protein.[10] gp3 also greatly enhances the efficiency and selectivity of DNA packaging in bulk *in vitro*.[44] In phage P22, the small terminase subunit gp3 is shown to bind DNA in a sequence independent manner and is a globular decamer in solution with a central annulus that can fit the DNA.[59] In the phage λ small terminase subunit gpNu1, the NMR structure shows a HTH motif for DNA binding,[73] and the T4 gp16 small terminase also has a predicted HTH motif, whereas gp3 of ϕ29 lacks a HTH motif.[74] The general strategy for genome packaging is thus retained in ϕ29 despite the apparent divergence from the conventional model with active participation of pRNA in the packaging motor function.

gp16 supercoils the DNA-gp3 packaging substrate in a reaction that is dependent upon gp3 covalently bound at the DNA termini.[21] This supercoiled DNA-gp3/gp16 complex is preferentially packaged into proheads *in vitro*. Thus, the description here of a stable and active prohead/pRNA/gp16 complex that can package DNA without additional gp16 (Figure 6) represents an alternative pathway of gp16 assembly and packaging initiation. Notably, however, this prohead/pRNA/gp16 intermediate was also capable of supercoiling DNA-gp3, just as demonstrated earlier with gp16 on free DNA-gp3 in the absence of proheads (Figure 9).[21] Figure 10 illustrates the alternative pathways for producing the prohead/pRNA/gp16/DNA-gp3 packaging initiation complex. To directly observe the events of initiation and progression of DNA-gp3 packaging *in vitro*, various mixtures of the proheads/pRNA, gp16 and DNA-gp3, without or with ATP, or complexes stalled in the packaging process with γS-ATP at different times, were prepared in BAC films,[75] mounted on support films, rotary metal shadowed and observed by transmission electron microscopy (data not shown). DNA in the process of packaging appeared to be supercoiled and condensed, but the provisional results have not yet provided a clear picture of the structure of the initiation complex or the progression of packaging. In another attempt to determine the pathway and events in packaging initiation, proheads and DNA-gp3 were isolated at times ranging from 45 to 90 min from a lysate of a restrictive infection of *B. subtilis* with the ϕ29 mutant *sus*14 (1241) that provides delayed lysis. gp16 was found in multiple copies on both the DNA-gp3 and the proheads (data not shown). The wrapping of supercoiled DNA by the free ϕ29 head-tail connector to remove negative supercoils[76] is a provocative reminder that the initiation of packaging may involve DNA-protein transactions within the motor that have not been contemplated. Further experimentation is needed to dissect the details of packaging initiation.

Isolation of the prohead-pRNA-gp16 motor assembly intermediate has facilitated single molecule studies that allow DNA translocation to be measured from initiation to completion, allowing study of the previously uncharacterized early steps of packaging and the demonstration of packaging forces >100 pN.[4, 77] Prohead/pRNA/gp16 assembly intermediates were attached to one bead, biotinylated DNA molecules were tethered to streptavadin-coated microspheres, and packaging was initiated by bringing the beads into contact in the presence of ATP. In these single molecule studies, gp3 is not required, whereas DNA without gp3 is packaged an order of magnitude less efficiently in bulk.[44] The prohead/pRNA/gp16 complex and DNA are rapidly brought into close physical contact in the laser tweezers, possibly bypassing the need for gp3. It is also noteworthy that use of DNA-gp3 in the single molecule studies results in great variation in DNA tether length upon initiation, indicating that the DNA-gp3 molecules have a higher order structure.[4]

Materials and Methods

Purification of DNA-gp3

DNA-gp3 and [^{3}H]DNA-gp3 were isolated from lysates of *Bacillus subtilis* RD2 (*sup*$^-$) infected with the mutant *sus*4(369)-*sus*8(22), defective for late transcription and production of the major capsid protein, respectively, as described.[21] Proteinase K-treated DNA, further purified in an isopycnic cesium chloride density gradient, was used to generate a *Hpa*I digest, which was phenol extracted and used for the EMSA determination of gp16 binding.

Preparation of proheads

Proheads with 174-base pRNA were purified from a lysate of *Bacillus subtilis* SpoOA12 (*sup*$^-$) cells infected with the mutant *sus*16(300)-*sus*14(1241) that is defective for the DNA packaging ATPase gp16 as described previously.[30]

Production and purification of soluble gp16 from *Bacillus subtilis*

The purified E/D segment of ϕ29 DNA-gp3 containing gene 16 was obtained by partial digestion with *Eco*RI[42] and cloned into the plasmid pUB18 that encodes kanamycin resistance. The sucrose inducible promoter SACB[43] was inserted before gp16 gene and the resulting pSACB-gp16 plasmid moved into *Bacillus subtilis* WB30 (asporogenic and protease negative) by protoplast transformation[78]. The maximum yield of the soluble protein (10 mg/liter) was obtained after induction of gene16 expression with 2% sucrose for 3 hr at 37°C. The expression of gp16 in *B. subtilis* did not result in inclusion body formation as in *E coli*,[20] and about 70% of the protein was found in the soluble fraction (supernatant). Sucrose-induced cells were passed through a French press twice in a buffer containing 50 mM Tris-HCl (pH 7.8), 200 mM NaCl, 5% glycerol and 2 mM TCEP. The lysate was clarified by centrifugation at 10,000 rpm for 15 min at 4°C in a SS-34 rotor. The supernatant was subjected to P11 phosphocellulose (Whatman) cation-exchange chromatography. The P11 column was equilibrated with lysis buffer, washed with 8 bed volumes of 300 mM NaCl in 50 mM Tris-HCl (pH 7.8), 5% glycerol and 2 mM TCEP, and gp16 was eluted with 350 mM NaCl in the same buffer. The P11 eluate containing gp16 was further purified on a hydroxyapatite column (Biorad), which was equilibrated with 300 mM NaCl in 50 mM Tris-HCl (pH 7.8), 5% glycerol and 2 mM TCEP. The column was washed with 3 bed volumes of 100 mM sodium phosphate (pH 6.8), 5% glycerol and 2 mM TCEP, followed by two bed volumes of 50 mM sodium phosphate (pH 6.8) in the same buffer. The protein was eluted by a ten-bed volume gradient of 100 mM to 900 mM NaCl in 50 mM sodium phosphate (pH 6.8), 5% glycerol and 2 mM TCEP. Fractions were analyzed by SDS-PAGE, and peak fractions containing pure gp16 were stored in aliquots at −70°C. The identity of the protein was confirmed by a Western blot developed with polyclonal anti-gp16 serum. The average yield of the purified gp16 was 8 mg/liter of culture.

In vitro DNA-gp3 packaging

Packaging in the defined *in vitro* system was performed as described.[44] DNA-gp3 (1μg) and proheads were mixed in the ratio of 1:2 in a total volume of 20 μl in 0.5X TMS buffer [25 mM Tris-HCl (pH 7.8), 5 mM MgCl2 and 50 mM NaCl] containing 0.5 mM ATP. Generally 15 copies (molecules) of gp16 per prohead were added and the mixture incubated at ambient temperature for 15 min. The gp16 copy number varied as indicated. DNase I was added to 1 μg/ml to digest the unpackaged DNA, while the packaged DNA was protected in the head. The DNase was inhibited and the packaged DNA extracted from the filled heads by adding EDTA to 25 mM and proteinase K to 500 μg/ml, and the efficiency of packaging was quantified following electrophoresis on a 0.8% agarose gel run in TBE buffer [89 mM Tris (pH 8.3), 89 mM Boric acid and 2.5 mM EDTA].

Sedimentation equilibrium

Sedimentation equilibrium experiments were performed with purified gp16 equilibrated in a buffer containing 50 mM sodium phosphate (pH 6.8), 400 mM NaCl and 2 mM TCEP at 4°C. Two samples at each concentration of 0.2, 0.4 and 0.8 mg/ml were analyzed in an An50Ti rotor in a Beckman Optima XL-I analytical centrifuge. Data was collected at 280 nm and at three rotor speeds of 5,000, 8,000 and 11,000 rpm. Equilibrium was reached when scans taken 4 hr apart were super-imposable. Each data curve was the result of at least three averaged scans. Partial specific volume (υ) for gp16 calculated from the primary amino acid sequence using SEDNTERP[79] was 0.7373 ml/g. Based on the primary amino acid sequence, the calculated monomer molecular weight of gp16 was 38,965 daltons. Using SEDNTERP, the calculated density (σ) of the buffer was 1.02859 g/ml and the viscosity (η) was 0.0167043.

Data were initially fit to a self-association model using NONLIN,[46] which yielded molecular weights suggestive of a trimer. Additional species that were included as fits were not good for a simple monomer to trimer model. The data at lower centrifugation speeds and higher protein concentrations were fit using SEDPHAT.[47] gp16 forms larger molecular weight species that are not reversible and are lost to the bottom of the cell. To determine the amount of loss, the area of absorbance for each cell was determined at each centrifuge speed relative to the initial absorbance at 3,000 rpm. This amounted to loss of 40% of the gp16 at 0.2–0.4 mg/ml and 65% loss at 0.8 mg/ml. The protein remaining in solution was fit as described above.

Gel filtration

Gel filtration was performed using a Superdex 200 HR 10/30 (Amersham Pharmacia Biotech) column at 4°C in a buffer containing 50 mM sodium phosphate (pH 6.8), 400 mM NaCl and 2 mM TCEP on an Akta-FPLC system (Amersham Pharmacia Biotech). Molecular weight standards were analyzed in the same buffer and contained, in kDa, thyroglobulin (669), human IgG (158), ovalbumin (44), myoglobin (17.6) and vitamin B12 (1.4).

Transmission electron microscopy

Glow discharge treated holey carbon films on 400 mesh copper grids were floated on samples of purified gp16 [50 μg/ml in 50 mM PIPES (pH 6.8) and 400 mM NaCl], negatively stained with 2% (w/v) uranyl acetate and imaged at 57,000 X magnification. Micrographs were made with a Philips EM301 electron microscope. The diameter of gp16 particles from the electron micrographs was determined by the use of Image J (NIH). Calibration was done from micrographs of a carbon-grating replica (Fullam, NY).

Preparation of pRNA

120-base and 106-base pRNA forms were generated by *in vitro* T7 transcription from pRT72 plasmid linearized with *Dde*I and *Apa*LI and (Invitrogen), respectively, as described.[33]

Alternatively, 120-base pRNA was produced from *in vitro* transcription of the *Bam*HI-linearized pH120RNAH plasmid (Atz et al., unpublished results). The 71-base pRNA expression construct pH71RNAH was generated by two rounds of PCR from the pRNA gene and by adding hammerhead ribozyme sequences to both ends of the template to generate uniform pRNA ends. The plasmid was cloned into pUC19 and transformed into *E.coli* DH5α The purified plasmid was linearized with *Sma*I and transcribed *in vitro* to obtain the 71-base pRNA. R7-pRNA was generated from *Bacillus subtilis* 12A (pUM102) as described.[33] All forms of pRNA were purified by electrophoresis in denaturing urea-acrylamide gels.[80] Individual pRNA bands were located by UV shadowing over polyethyleneimine UV_{254}-cellulose plates with a 254 nm light source. pRNA bands were excised and the pRNA eluted twice by diffusion into TEN buffer [10mM Tris-HCl (pH 8.0), 1mM EDTA and 100 mM NaCl] for 3 hr at 4°C.

Electrophoretic mobility shift assay

120-base pRNA was incubated with increasing concentrations of gp16 in 50 mM Tris- HCl (pH 7.8), 10 mM $MgCl_2$ and 100 mM NaCl for 20 min at room temperature. 5% glycerol, 0.05% bromophenol blue and 0.05% xylene cyanol were added to each reaction, the complexes were resolved by electrophoresis in a 0.8% agarose gel in TB buffer [89 mM Tris-HCl (pH 8.3) and 89 mM Boric acid] for 3 hr, and the gels were stained with ethidium bromide. EMSA was also performed with *Hpa*I-digested ϕ29 DNA fragments and gp16 in a similar manner.

Preparation of RNA-free proheads

Purified proheads were diluted 10-fold in TMS buffer and digested with 1μg/ml of RNase A for 15 min at room temperature.[44] These RNA-free proheads were purified on a 10–40% sucrose density gradient in TMS buffer (50 mM Tris-HCl (pH 7.8), 10 mM $MgCl_2$ and 100 mM NaCl) by centrifugation for 3hr at 35,000 rpm in a SW55 rotor. The prohead band was collected and the particles pelleted in TMS buffer.

Reconstitution of pRNA-free proheads with pRNA

Ten copies of the pRNA produced from *in vitro* transcription were used per prohead and the mixture incubated for 10 min at room temperature for reconstitution. These reconstituted proheads were repurified on a sucrose gradient to remove excess pRNA.

Isolation of the prohead/pRNA/gp16 ATPase motor assembly intermediate

Proheads with 174-base pRNA and gp16 were incubated in TMS buffer without ATP at ambient temperature for 20 min at a ratio of 20 gp16 molecules per prohead. After incubation, the reaction mixture was loaded on a 5–20% sucrose gradient in TM buffer [50 mM Tris-HCl (pH 7.6) and 5 mM $MgCl_2$] and centrifuged at 35,000 rpm for 30 min in a SW55 rotor at 4°C. The peak band was collected with a syringe and 20 μl used for testing the *in vitro* DNA-gp3 packaging activity upon addition of DNA-gp3 and ATP. 100 μl of the fraction was precipitated with 10% TCA and subjected to SDS-PAGE to determine the composition of the prohead/pRNA/gp16 intermediate. pRNA-free proheads and proheads reconstituted with various forms of pRNA with A-helix deletions (71-base, 106-base and R7-pRNA (Fig4(b)–(d)) were used to screen for binding of gp16 as described above.

RNase footprinting

120-base pRNA was 5′-labeled with Optikinase™ (USB Corp) and [γ-^{32}P]ATP after removal of the 5′ terminal phosphate with shrimp alkaline phosphatase. The end-labeled pRNA was further purified by electrophoresis in denaturing urea-acrylamide gels. The pRNA bands were eluted from the gel into TEN buffer and concentrated by isopropanol precipitation. pRNA

obtained after precipitation was used for footprinting and reconstitution of pRNA-free proheads for footprinting.

140 μg of pRNA-free proheads were reconstituted with 2.8 μg of 5′ end-labeled 120-base pRNA (6 pRNA/prohead; 7×10^5 CPM/μg of pRNA) in TM buffer for 20 min at room temperature. Proheads were separated from the unbound pRNA by dilution into 5 ml TM buffer and pelleting at 35,000 rpm for 5 hr in the SW55 rotor at 4°C as described.[26]

Prohead-bound [^{32}P]pRNA, [^{32}P]pRNA alone (2×10^4 CPM) and [^{32}P]pRNA complexed with gp16 were digested with varying concentrations of RNase A (Ambion), RNase T1 or RNase V1(Ambion) in 10 μl reactions for 15 min at ambient temperature. pRNA was extracted with 200 μl of a mixture containing 1 part 50 mM Tris-HCl (pH 7.6), 10 mM EDTA, 20μg/ml yeast tRNA (Ambion) and 1 part phenol. The aqueous phases were precipitated with 0.6 volumes of isopropanol containing 20 μg/ml glycogen. Pellets were resuspended in 4 M urea, 20% glycerol, 0.05% xylene cyanol and 0.05% bromophenol blue and run on a 10% denaturing 8.3 M urea polyacrylamide gel.

Cryo-electron microscopy

Proheads with 174-base pRNA and prohead/174-base pRNA/gp16 particles were flashfrozen on holey grids in liquid ethane. Images were recorded at 39,000X magnification with a CM200 FEG microscope, with electron dose levels of approximately 20 $e^-/Å^2$. All micrographs were digitized at 4.24 Å pixel^{-1} using a Zeiss SCAI scanner.

Individual particle images were boxed, floated, and preprocessed to normalize mean intensities and variances and to remove linear background gradients. Reference projections of a previously published prohead reconstruction[30] were used to initially classify particles for three-dimensional reconstruction. The resulting model was used to recalculate reference projections for better particle classification. Several cycles of iterative particle classification and reconstruction were performed until convergence had been reached. Structure factor phases and amplitudes were modified as indicated by the parameters of the contrast transfer function. All steps of the reconstruction process, including determination of the contrast transfer function parameters, were performed with the program EMAN.[81] Five-fold symmetry was assumed in the reconstruction. The number of particles incorporated in the final reconstruction was 1705, and the final resolution of the reconstruction was 18.5 Å, as determined by the Fourier shell correlation method using a correlation coefficient of 0.5 between independent half data sets as the cut-off criterion.

Sedimentation assay of DNA-gp16 and DNA-prohead/pRNA/gp16

[^{3}H]DNA-gp3 (1μg) was diluted in water and heated for 5 min at 37°C. A 0.1 volume of 10x TM buffer and 12 copies of gp16 per DNA were added to give a final reaction volume of 100 μl. The mixture was incubated at ambient temperature for 10 min and then centrifuged in a 5–20% linear sucrose density gradient containing TM [50 mM Tris-HCl (pH 7.6), 5 mM NaCl] buffer in the SW55 rotor at 35,000 rpm for 2 hr at 20°C. Fractions were collected and the [^{3}H]DNA-gp3 quantified by liquid scintillation counting. Also, samples of the fractions were treated with 5μg/ml DNase I at room temperature for 20 min, and dot-blots of the samples were developed with gp16-antiserum. As a control, gp16 alone was sedimented on a sucrose gradient and samples of the fractions used for dot-blots and gp16 quantification. Prohead/pRNA/gp16 complexes (12 copies of gp16 per prohead) were prepared, incubated with [^{3}H]DNA-gp3, and sedimented in a sucrose gradient to study their activity in binding and supercoiling DNA-gp3 as described.[21]

Extract preparation

B. subtilis SpoOA12 (*sup*$^{-}$) was infected with the mutant *sus*7(614)-*sus*8(769)-*sus*14(1241) that is defective for the prohead scaffold and capsid proteins and is a source of gp16, and extracts of these infected cells were prepared as described.[16]

Abbreviations used

pRNA, prohead RNA; gp, gene product; cryo-EM, cryo-electron microscopy; EMSA, electrophoretic mobility shift assay..

Acknowledgements

We thank Siddhartha Jena for DLS analysis, Steve Erickson and Rockney Atz for technical assistance, Daniel Cohen and Charlene Peterson for expertise with figures. M.C.M was supported by NSF grant MCB-0443899. This research was supported by NIH grants DE-003606 and GM-059604.

References

1. Catalano, CE. Viral genome packaging machines: an overview. In: Catalano, CE., editor. Viral genome packaging machines: Genetics, structure and mechanism. Georgetown, TX: 2005. p. 1-4.Landes Bioscience/Eurekah.com
2. Jardine, PJ.; Anderson, DL. DNA packaging in double-stranded DNA phages. In: Calendar, R., editor. The bacteriophages. New York: oxford press; 2006. p. 49-65.
3. Smith DE, Tans SJ, Smith SB, Grimes S, Anderson DL, Bustamante C. The bacteriophage phi29 portal motor can package DNA against a large internal force. Nature (London) 2001;413:748–752. [PubMed: 11607035]
4. Rickgauer JP, Fuller N, Grimes S, Jardine PJ, Anderson DL, Smith DE. Portal motor velocity and internal force resisting viral DNA packaging in bacteriophage phi29. Biophys. J 2008;94:159–167. [PubMed: 17827233]
5. Murialdo H, Becker A. Head morphogenesis of complex double-stranded deoxyribonucleic acid bacteriophages. Microbiol. Rev 1978;42:529–576. [PubMed: 362149]
6. Earnshaw WC, Casjens SR. DNA packaging by the double-stranded DNA phages. Cell 1980;21:319–331. [PubMed: 6447542]
7. Feiss M. Terminase, a viral enzyme involved in the recognition, cutting and packaging of bacteriophage λ chromosomes. Trends genet 1986;2:100–104.
8. Mitchell MS, Matsuzaki S, Imai S, Rao VB. Sequence analysis of bacteriophage T4 DNA packaging/terminase genes 16 and 17 reveals a common ATPase center in the large subunit of viral terminases. Nucl. Acids. Res 2002;30:4009–4021. [PubMed: 12235385]
9. Sun S, Kondabagil K, Gentz PM, Rossmann MG, Rao VB. The structure of the ATPase that powers DNA packaging into bacteriophage T4 procapsids. Mol. Cell 2007;25:943–949. [PubMed: 17386269]
10. Guo P, Peterson C, Anderson DL. Prohead and DNA-gp3 dependent ATPase activity of the DNA packaging protein gp16 of bacteriophage ϕ29. J. Mol. Biol 1987;197:229–236. [PubMed: 2960820]
11. Fujisawa H, Shibata H, Kato H. Analysis of interactions among factors involved in the bacteriophage T3 DNA packaging reaction in a defined *in vitro* system. Virol 1991;185:788–794.
12. Kanamaru S, Kondabagil K, Rossmann MG, Rao VB. The functional domains of bacteriophage T4 terminase. J. Biol. Chem 2004;279:40795–40801. [PubMed: 15265872]
13. Kondabagil K, Zhang Z, Rao VB. The DNA translocating ATPase of bacteriophage T4 packaging motor. J. Mol. Biol 2006;363:786–799. [PubMed: 16987527]
14. Feiss, M.; Catalano, CE. Bacteriophage Lambda terminase and the mechanism of viral DNA packaging. In: Catalano, CE., editor. Viral genome packaging machines: Genetics, structure and mechanism. Georgetown, TX: 2005. p. 5-39.Landes Bioscience/Eurekah.com
15. Guo P, Peterson C, Anderson DL. Initiation events in *in-vitro* packaging of bacteriophage ϕ29 DNA-gp3. J. Mol. Biol 1987;197:219–228. [PubMed: 3119862]

16. Bjornsti MA, Reilly BE, Anderson DL. In vitro assembly of the *Bacillus subtilis* bacteriophage ϕ29. Proc. Natl.Acad. Sci. USA 1981;78:5861–5865. [PubMed: 6795639]

17. Bjornsti MA, Reilly BE, Anderson DL. Morphogenesis of bacteriophage ϕ29 of *Bacillus subtilis*: oriented and quantized *in vitro* packaging of DNA-gp3. J. Virol 1983;45:383–396. [PubMed: 6185695]

18. Simpson AA, Tao Y, Leiman PG, Badasso MO, He Y, Jardine PJ, Olson NH, Morais MC, Grimes S, Anderson DL, et al. Structure of the bacteriophage phi29 DNA packaging motor. Nature 2000;408:745–750. [PubMed: 11130079]

19. Gausch A, Pous J, Ibarra B, Gomis-Ruth FX, Valpuesta JM, Sousa N, Carrascosa JL, Coll M. Detailed architecture of a DNA translocating machine: the high-resolution structure of the bacteriophage ϕ29 connector particle. J. Mol. Biol 2002;315:663–676. [PubMed: 11812138]

20. Guo P, Grimes S, Anderson DL. A defined system for *in vitro* packaging of DNA-gp3 of the *Bacillus subtilis* bacteriophage ϕ29. Proc. Natl. Acad. Sci. USA 1986;83:3505–3509. [PubMed: 3458193]

21. Grimes S, Anderson DL. The bacteriophage ϕ29 packaging proteins supercoil the DNA ends. J. Mol. Biol 1997;266:901–914. [PubMed: 9086269]

22. Guo P, Erickson S, Anderson DL. A small viral RNA is required for *in vitro* packaging of bacteriophage ϕ29 DNA. Science 1987a;236:690–694. [PubMed: 3107124]

23. Atz R, Ma S, Gao J, Anderson DL, Grimes S. Alanine scanning and FE-BABE probing of the bacteriophage ϕ29 prohead RNA-connector interaction. J. Mol. Biol 2007;369:239–248. [PubMed: 17433366]

24. Grimes S, Anderson DL. RNA dependence of the bacteriophage ϕ29 DNA packaging ATPase. J. Mol. Biol 1990;215:559–566. [PubMed: 1700132]

25. Wichitwechkarn J, Bailey S, Bodley JW, Anderson DL. Prohead RNA of bacteriophage ϕ29: size, stoichiometry and biological activity. Nucl Acids Res 1989;17:3459–3468. [PubMed: 2498842]

26. Reid RJ, Bodley JW, Anderson DL. Characterization of the prohead-pRNA interaction of bacteriophage ϕ29. J. Biol. Chem 1994;269:5157–5162. [PubMed: 8106496]

27. Trottier M, Guo P. Approaches to determine stoichiometry of viral assembly components. J. Virol 1997;71:487–494. [PubMed: 8985375]

28. Ibarra B, Caston JR, Llorca O, Valle M, Valpuesta JM, Carrascosa JL. Topology of the components of the DNA packaging machinery in the phage ϕ29 prohead. J. Mol. Biol 2000;298:807–815. [PubMed: 10801350]

29. Morais MC, Tao Y, Olson NH, Grimes S, Jardine PJ, Anderson DL, Baker TS, Rossmann MG. Cryoelectron-microscopy image reconstruction of symmetry mismatches in bacteriophage ϕ29. J. Struct. Biol 2001;135:38–46. [PubMed: 11562164]

30. Morais MC, Choi KH, Koti JS, Chipman PR, Anderson DL, Rossmann MG. Conservation of capsid structure in tailed dsDNA bacteriophages: the pseudoatomic structure of ϕ29. Mol. Cell 2005;18:149–159. [PubMed: 15837419]

31. Shu D, Zhang H, Jin J, Guo P. Counting of six pRNAs of phi29 DNA packaging motor with customized single-molecule dual-view system. EMBO. J 2007;26:527–537. [PubMed: 17245435]

32. Grimes S, Jardine PJ, Anderson DL. Bacteriophage phi29 DNA packaging. Adv. Virus Res 2002;58:255–294. [PubMed: 12205781]

33. Reid RJ, Bodley JW, Anderson DL. Identification of bacteriophage ϕ29 prohead RNA domains necessary for in vitro DNA-gp3 packaging. J. Biol. Chem 1994;269:9084–9089. [PubMed: 8132646]

34. Reid RJ, Zhang F, Benson S, Anderson DL. Probing the structure of bacteriophage ϕ29 prohead RNA with specific mutations. J. Biol. Chem 1994;269:18656–18661. [PubMed: 8034614]

35. Zhang C, Lee CS, Guo P. The proximate 5′ and 3′ ends of the 120-base viral RNA (pRNA) are crucial for the packaging of bacteriophage phi29. Virol 1994;201:77–85.

36. Zhang C, Garver K, Guo P. Inhibition of phage phi29 assembly by antisense oligonucleotides targeting viral pRNA essential for DNA packaging. Virol 1995;211:568–676.

37. Chemla YR, Aathavan K, Michaelis J, Grimes S, Jardine PJ, Anderson DL, Bustamante C. Mechanism of force generation of a viral DNA packaging motor. Cell 2005;122:683–692. [PubMed: 16143101]

38. Hendrix RW. Symmetry mismatch and DNA packaging in large bacteriophages. Proc. Natl. Acad. Sci. USA 1978;75:4779–4783. [PubMed: 283391]

39. Baumann RG, Mullaney J, Black LW. Portal fusion protein constraints on function in DNA packaging of bacteriophage T4. Mol. Microbiol 2006;61:16–32. [PubMed: 16824092]
40. Hugel T, Michaelis J, Hetherington CL, Jardine PJ, Grimes S, Walter JM, Falk W, Anderson DL, Bustamante C. Experimental test of connector rotation during DNA packaging into bacteriophage phi29 capsids. PLoS Biol 2007;5:e59. [PubMed: 17311473]
41. Lebedev AE, Krause MH, Isidro AL, Vagin AA, Orlova EV, Turner J, Dodson EJ, Tavares P, Antson AA. Structural framework for DNA translocation via the viral portal protein. EMBO. J 2007;26:1984–1994. [PubMed: 17363899]
42. Garvey KJ, Saedi MS, Ito J. The complete sequence of *Bacillus* phage ϕ29 gene16: a protein required for the genome encapsidation reaction. Gene 1985;40:311–316. [PubMed: 3879485]
43. Li M, Wong SL. Cloning and characterization of the GROESL operon from *Bacillus subtilis*. J. Bacteriol 1992;174:3981–3992. [PubMed: 1350776]
44. Grimes S, Anderson DL. *In vitro* packaging of bacteriophage ϕ29 DNA restriction fragments and the role of the terminal protein gp3. J. Mol. Biol 1989;209:91–100. [PubMed: 2530357]
45. Bjornsti MA, Reilly BE, Anderson DL. Bacteriophage ϕ29 proteins required for *in vitro* DNA-gp3 packaging. J. Virol 1984;50:766–772. [PubMed: 6427474]
46. Johnson M, Correia JJ, Yphantis DA, Halvorson H. Analysis of data from the analytical ultracentrifuge by nonlinear least-squares techniques. Biophys. J 1981;36:575–588. [PubMed: 7326325]
47. Vistica J, Dam J, Balbo A, Yikilmaz E, Mariuzza RA, Rouault TA, Schuck P. Sedimentation equilibrium analysis of protein interactions with global implicit mass conservation constraints and systematic noise decomposition. Anal. Biochem 2004;326:234–256. [PubMed: 15003564] SEDPHAT: freeware from www.analyticalultracentrifugation.com
48. Ibarra B, Valpuesta J, Carrascosa JL. Purification and functional characterization of p16, the ATPase of the bacteriophage ϕ29 packaging machinery. Nucl. Acid. Res 2001;29:4264–4273.
49. Lee T, Guo P. Interaction of gp16 with pRNA and DNA for genome packaging by the motor of bacterial virus phi29. J. Mol. Biol 2006;356:589–599. [PubMed: 16376938]
50. Guo P, Bailey S, Bodley JW, Anderson DL. Characterization of the small RNA of the bacteriophage ϕ29 DNA packaging machine. Nucl. Acid. Res 1987d;15:7081–7090.
51. Bailey S, Wichitwechkarn J, Johnson D, Reilly BE, Anderson DL, Bodley JW. Phylogenetic analysis and secondary structure of the *Bacillus subtilis* bacteriophage RNA required for DNA packaging. J. Biol. Chem 1990;265:22365–22370. [PubMed: 2125049]
52. Przech AJ, Yu D, Weller SK. Point mutations in exon I of the herpes simplex virus putative terminase subunit, UL15, indicate that the most conserved residues are essential for cleavage and packaging. J.Virol 2003;77:9613–9621. [PubMed: 12915573]
53. Huang LP, Guo P. Use of PEG to acquire highly soluble DNA-packaging enzyme gp16 of bacterial virus phi29 for stoichiometry quantification. J. Virol. Methods 2003;109:235–244. [PubMed: 12711068]
54. Draper B, Rao BV. An ATP hydrolysis sensor in the DNA packaging motor from bacteriophage T4 suggests an inch-type translocation mechanism. J. Mol. Biol 2007;369:79–94. [PubMed: 17428497]
55. Gual A, Camacho AG, Alonso CJ. Functional analysis of the terminase large subunit, G2P, of *Bacillus subtilis* Bacteriophage SPP1. J. Biol.Chem 2000;275:35311–35319. [PubMed: 10930407]
56. Leffers G, Rao VB. Biochemical characterization of an ATPase activity associated with the large packaging subunit gp17 from bacteriophage T4. J. Biol. Chem 2000;275:37127–37136. [PubMed: 10967092]
57. Paris W, Rubinchik S, Yang Y, Gold M. A new procedure for the purification of bacteriophage λ terminase enzyme and its subunits. Properties of gene product A the large subunit. J. Biol. Chem 1994;269:13564–13574. [PubMed: 8175792]
58. Casjens, S.; Weigele, P. DNA packaging by bacteriophage P22. In: Catalano, CE., editor. Viral genome packaging machines: Genetics, structure and mechanism. Georgetown, TX: 2005. p. 80-88.Landes Bioscience/Eurekah.com
59. Nemecek D, Gilcrease EB, Kang S, Prevelige PE Jr, Casjens S, Thomas GJ Jr. Subunit conformations and assembly states of a DNA-translocating motor: The terminase of bacteriophage P22. J. Mol. Biol 2007;374:817–836. [PubMed: 17945256]

60. Serwer P. Evolution and the complexity of bacteriophages. Virol. J 2007;4:30–39. [PubMed: 17355641]
61. Morita M, Tasaka M, Fujisawa H. Structure and functional domains of the large subunit of the bacteriophage T3 DNA packaging enzyme: importance of the C-terminal region in prohead binding. J. Mol. Biol 1995;245:635–644. [PubMed: 7844832]
62. Eppler K, Wyckoff E, Goates J, Parr R, Casjens S. Nucleotide sequence of the bacteriophage P22 genes required for DNA packaging. Virol 1991;183:519–538.
63. Yeo A, Feiss M. Specific interaction of terminase, the DNA packaging enzyme of bacteriophage lambda, with the portal protein of the prohead. J. Mol. Biol 1995;245:141–150. [PubMed: 7799432]
64. Sippy J, Feiss M. Analysis of a mutation affecting the specificity domain for the prohead binding of the bacteriophage lambda terminase. J. Bacteriol 1992;174:850–856. [PubMed: 1531050]
65. Kainov DE, Pirttimaa M, Tuma R, Butcher SJ, Thomas GJJ, Bamford DH, Makeyev EV. RNA packaging device of double-stranded RNA bacteriophages, possibly as simple as hexamer of P4 protein. J. Biol. Chem 2003;278:48084–48091. [PubMed: 12966097]
66. Burroughs AM, Iyer LM, Aravind L. Comparative genomics and evolutionary trajectories of viral ATP dependent DNA-packaging systems. Gene and Prot. Evol 2007;3:48–65.
67. Iyer LM, Makarova KS, Koonin EV, Aravind L. Comparative genomics of the FtsK HerA superfamily of pumping ATPases: implications for the origins of chromosome segregation, cell division and viral capsid packaging. Nucl. Acid. Res 2004;32:5260–5279.
68. Massey TH, Mercogliano CP, Yates J, Sherratt DJ, Lowe J. Double-stranded DNA translocation: Structure and mechanism of hexameric FtsK. Mol. Cell 2006;23:457–469. [PubMed: 16916635]
69. Peng X, Basta T, Haring M, Garrett RA, Prangishvili D. Genome of Acidianus bottle-shaped virus and insights into the replication and packaging mechanisms. Virol 2007;364:237–243.
70. Zhang F, Lemieux S, Wu X, Arnaud SD, McMurray CT, Major F, Anderson DL. Function of hexameric RNA in packaging of bacteriophage ϕ29 DNA *in vitro*. Mol. Cell 1998;2:141–147. [PubMed: 9702201]
71. Guo P, Zhang C, Chen C, Garver K, Trottier M. Inter-RNA interaction of phage ϕ29 pRNA to form a hexameric complex for viral DNA transportation. Mol. Cell 1998;2:149–155. [PubMed: 9702202]
72. Chen C, Guo P. Sequential action of six virus-encoded DNA-packaging RNAs during phage ϕ29 genomic DNA translocation. J. Virol 1997;71:3864–3871. [PubMed: 9094662]
73. de Beer TD, Fang J, Ortega M, Yang Q, Maes L, Duffy C, Berton N, Sippy J, Overduin M, Feiss M, Catalano CE. Insights into specific DNA recognition during the assembly of a viral genome packaging machine. Mol. Cell 2002;9:981–991. [PubMed: 12049735]
74. Kamtekar S, Berman JA, Wang J, Lazaro MJ, Devega M, Blanco L, Salas M, Steitz TA. The ϕ29 DNA polymerase: protein-primer structure suggests a model for the initiation to elongation transition. EMBO J 2006;25:1335–1343. [PubMed: 16511564]
75. Vollenweider H, Sogo JM, Koller T. A routine method for protein free spreading of double and single stranded nucleic acid molecules. Proc. Natl. Acad. Sci. USA 1975;72:83–87. [PubMed: 164030]
76. Turnquist S, Simon M, Egelman E, Anderson D. Supercoiled DNA wraps around the bacteriophage ϕ29 head-tail connector. Proc. Natl. Acad. Sci. USA 1992;89:10479–10483. [PubMed: 1438237]
77. Fuller DN, Rickgauer JP, Jardine PJ, Grimes S, Anderson DL, Smith DE. Ionic effects on viral DNA packaging and portal motor function in bacteriophage ϕ29. Proc. Natl. Acad. Sci. USA 2007;104:11245–11250. [PubMed: 17556543]
78. Chang S, Cohen SNC. High frequency transformation of *Bacillus subtilis* protoplasts by plasmid DNA. Mol. Gen. Genetics 1979;168:111–115.
79. Laue, TM.; Shah, BD.; Ridgeway, TM.; Pelletier, SL. Analytical Ultracentrifugation in Biochemistry and Polymer Science. Harding, S.; Rowe, A.; Horton, J., editors. Cambridge: Royal Society of Chemistry; 1992. SEDNTERP: freeware from ww.jphilo.mailway.com
80. Wichitwechkarn J, Johnson D, Anderson DL. Mutant prohead RNAs in the *in vitro* packaging of bacteriophage ϕ29 DNA-gp3. J. Mol. Biol 1992;223:991–998. [PubMed: 1538407]
81. Ludtke SJ, Baldwin PR, Chiu W. EMAN: Semiautomated software for high resolution single-particle reconstructions. J. Struct.Biol 1999;128:82–97. [PubMed: 10600563]

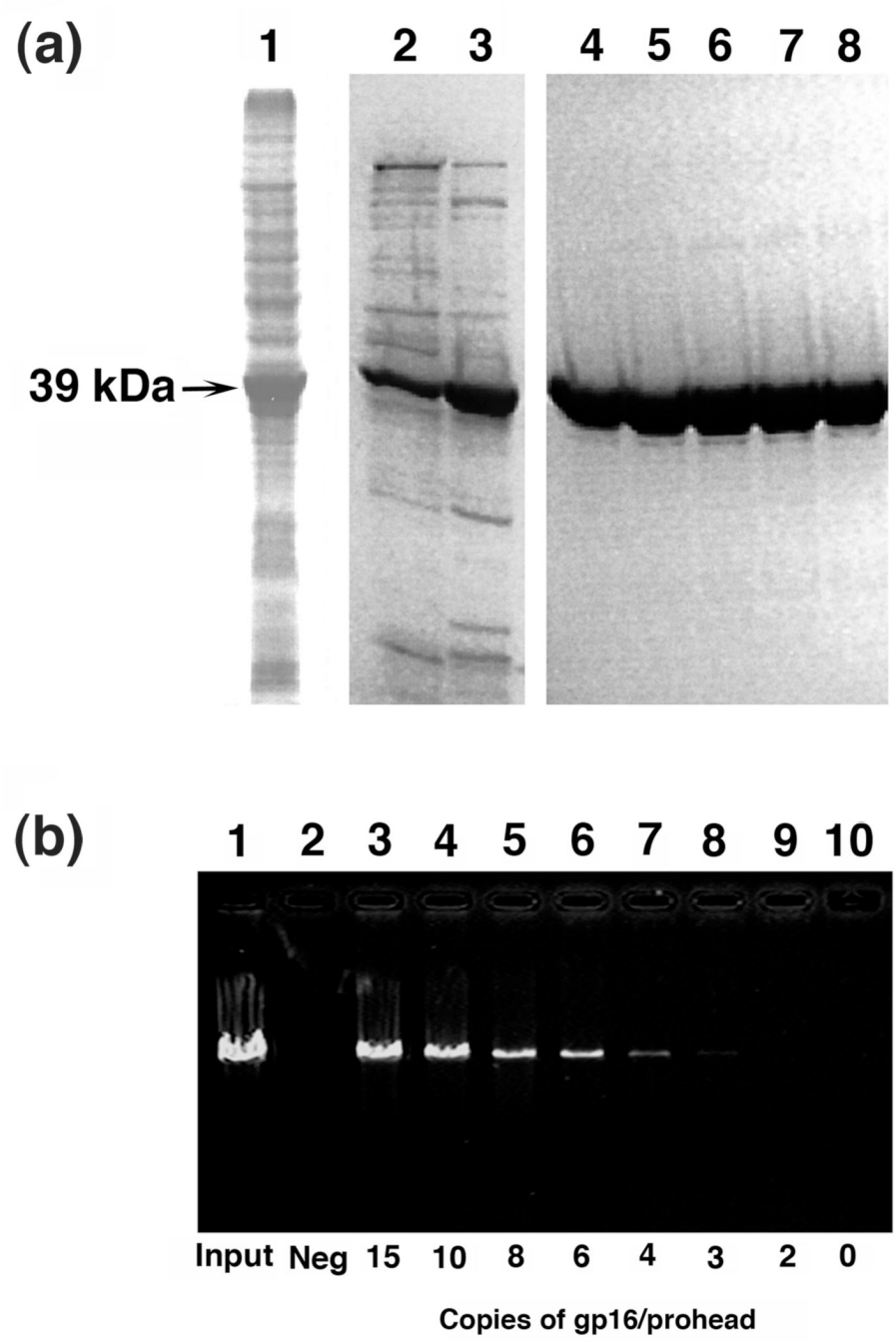

Figure 1.

Purification and *in vitro* DNA-gp3 packaging activity of the ATPase gp16. (a) SDS-PAGE of samples from steps in the purification of gp16 following expression in *Bacillus subtilis* (pSACB-gp16). The lanes show: 1) the supernatant from the cell lysate; 2–3) P11 cation exchange column peak fractions; 4–8) hydroxyapatite column peak fractions. (b) Packaging activity of purified gp16 determined by the *in vitro* DNA-gp3 packaging assay (Methods). The lanes show: 1) the input DNA-gp3 added to the reaction; 3–9) DNA that was packaged in the presence of 15, 10, 8, 6, 4, 3 and 2 copies (molecules) of gp16 per prohead, respectively; 2 and 10) negative controls in which ATP and gp16 were omitted, respectively, from the packaging reaction.

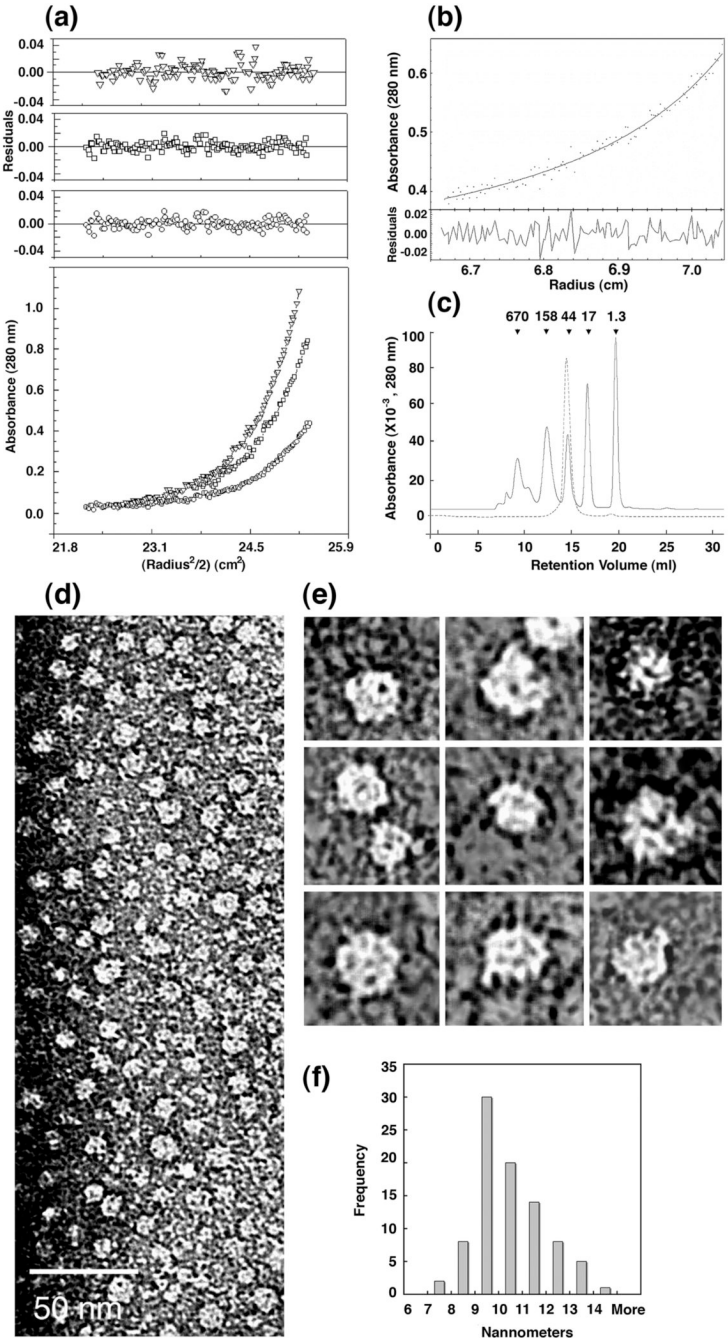

Figure 2.

Multimerization of the purified ATPase gp16. (a) Sedimentation equilibrium analysis of gp16 in 50 mM sodium phosphate (pH 6.8), 400 mM sodium chloride and 2 mM TCEP. Plots of protein concentration (A_{280}) versus radial position ($r^2/2$) at 11,000 rpm are shown at three different loading concentrations in the lower panel, and residuals of each set of data fit to a self association model are shown in the upper panels. (b) Species analysis of gp16 using SEDPHAT revealed that 80–85% of the protein was trimer and 15–20% was monomer at the lowest protein concentration, 0.2 mg/ml, analyzed at the highest speed of centrifugation, 11,000 rpm. Residuals to this fit are shown in the lower panel. At higher protein concentrations, analysis revealed predominantly trimers with varying amounts of monomer, hexamer and traces of

dodecamer (text). (c) Gel filtration elution profiles of proteins in the same buffer used for sedimentation equilibrium studies, plotted as protein concentration (A_{280}) versus retention volume (ml). The dashed line shows the elution profile of gp16 at approximately 100 μg/ml at the peak. The solid line shows the elution profile of MW standards with molecular weight (kDa) indicated across the top of the profile. (d) and (e) Transmission electron micrographs of gp16 negatively stained with 2% (w/v) uranyl acetate (Methods). (f) Histogram showing the measurement of the diameter of gp16 from electron micrographs (n = 88).

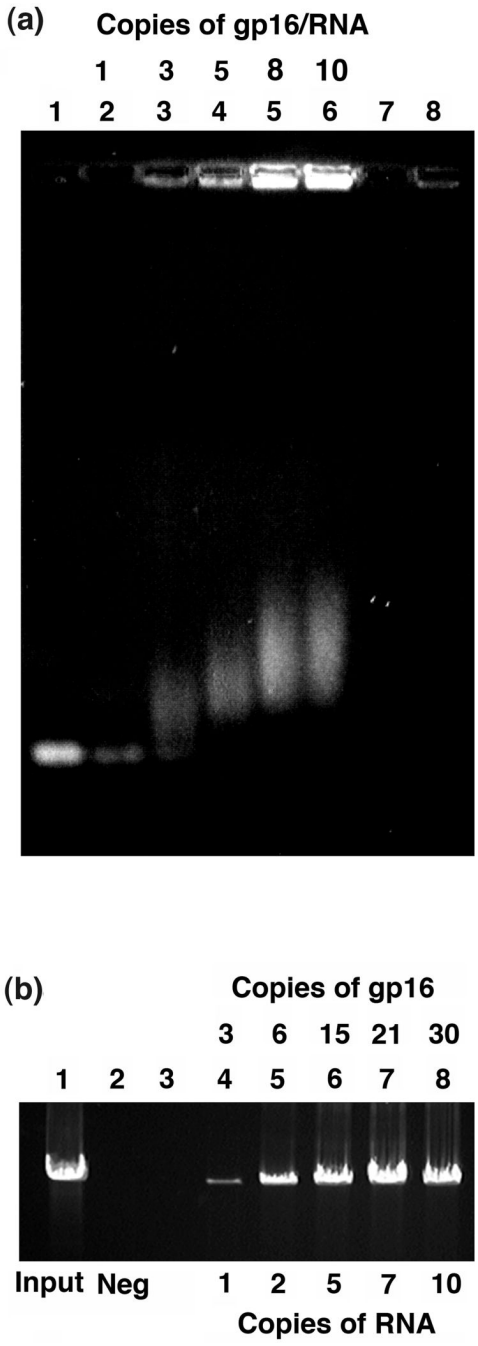

Figure 3.

Binding of gp16 to pRNA, and the activity of the pRNA-gp16 complex in *in vitro* DNA-gp3 packaging. (a) EMSA of 120-base pRNA incubated with increasing concentrations of gp16. The lanes show: 1) 120-base pRNA alone; 2–6) shift of pRNA in the presence of 1, 3, 5, 8 and 10 copies (molecules) of gp16 per pRNA molecule, respectively; 7) empty; 8) 10 copies of gp16 alone. (b) 120-base pRNA/gp16 (1:3) was added in increasing amounts to pRNA-free proheads and the mixtures tested for activity in the *in vitro* DNA-gp3 packaging assay. The lanes show: 1) input DNA-gp3 added to the reaction; 3) empty; 4–8) packaged DNA in the presence of pRNA:gp16 copies per prohead of 1:3, 2:6, 5:15, 7:21 and 10:30, respectively; 2) negative control without ATP

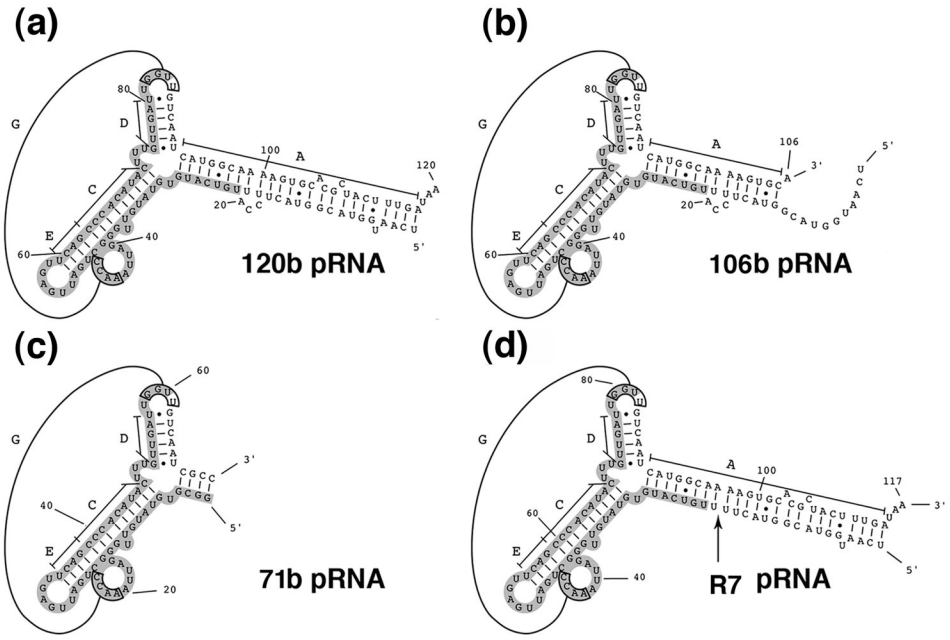

Figure 4.

Secondary structure prediction of various forms of pRNA tested for gp16 binding. (a) 120-base pRNA. (b) 106-base pRNA with a 14-base deletion at the 3′ end of the A-helix. (c) 71-base pRNA with a deletion of the A-helix. (d) R7-pRNA with deletion of the CCA bulge (bases 18–20), indicated by an arrow.

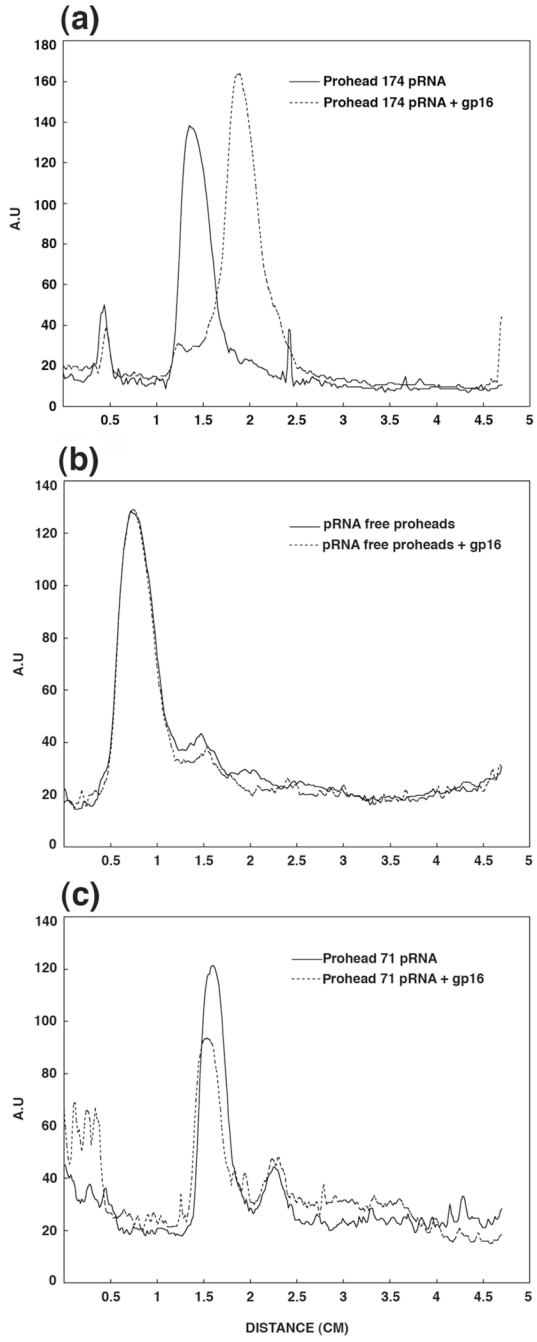

Figure 5.

The sedimentation rate of proheads/pRNA increased in the presence of gp16 and was dependent on the presence of the pRNA A-helix. (a) Sucrose density gradient centrifugation profiles of proheads/174-base pRNA (solid line) and proheads/174-base pRNA incubated with gp16 (dashed line). Sedimentation is from left to right. gp16 was bound to proheads containing 174-base pRNA in the faster sedimenting peak as revealed by SDS-PAGE (Figure 6 (a)) and by *in vitro* DNA-gp3 packaging (Figure 6(b)). (b) Sucrose density gradient profile of pRNA-free proheads (solid line) and pRNA-free proheads incubated with gp16 (dashed line), showing that gp16 did not alter the sedimentation rate of the pRNA-free proheads; gp16 was not found on these proheads by SDS-PAGE. (c) Sucrose density gradient profile of proheads /71-base pRNA

(solid line) and proheads/71-base pRNA incubated with gp16 (dashed line), showing that gp16 did not alter the sedimentation rate of these proheads; gp16 was not found on the particles. The gradients in a), b) and c) were run at different times and under different conditions, and the peak positions are not comparable.

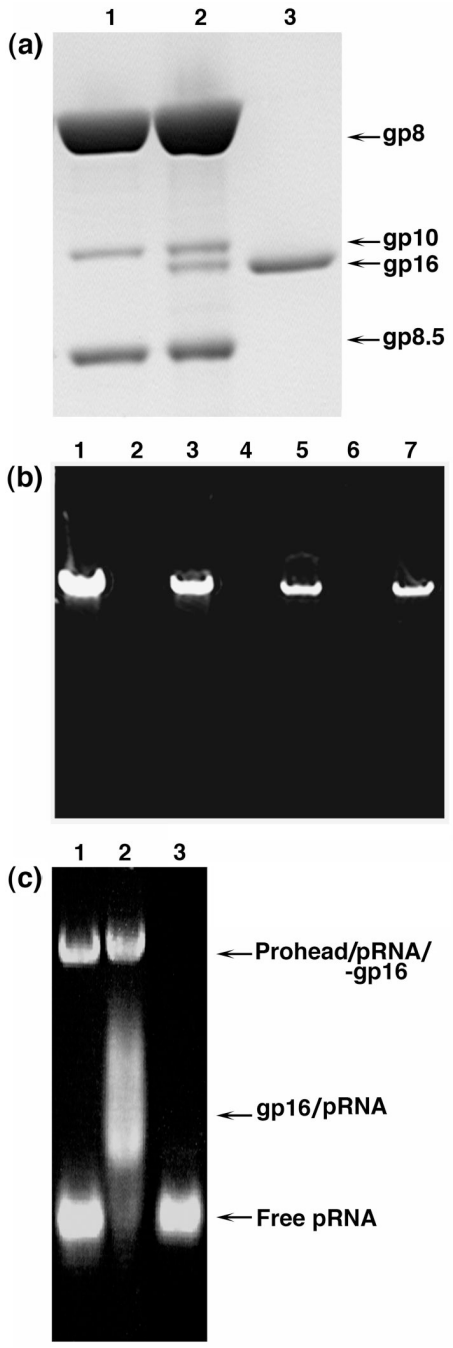

Figure 6.

Composition of the gradient-isolated prohead/pRNA/gp16 complex and its activity in *in vitro* DNA-gp3 packaging. (a) SDS-PAGE of peak sucrose gradient fractions from Figure 5 (a). The lanes show: 1) proheads/174-base pRNA; 2) proheads/174-base pRNA with bound gp16; 3) gp16 marker alone. (b) DNA packaging activity *in vitro* of the prohead/174-base pRNA/gp16 complex isolated from the sucrose gradient of Figure 5(a) upon addition of DNA-gp3 and ATP. The lanes show: 1) the input DNA in the packaging reaction; 5) DNA packaged by the gradient-isolated prohead/174-base pRNA/gp16 complex; 7) DNA packaged by the gradient-isolated prohead/pRNA/gp16 particle with 12 additional copies (molecules) of gp16 added per prohead; 4 and 6) negative controls in which ATP was omitted from the reaction;

3) packaging in which proheads/pRNA and gp16 were mixed and not sedimented; 2) ATP negative control for the reaction of lane 3. The prohead concentration was 2 times higher in the reaction of lane 3 than in the reactions of lanes 4–7 where the prohead/pRNA/gp16 complex was isolated from the sucrose gradient. (c) EMSA analysis of proheads/120-base pRNA incubated with gp16. The lanes show: 1) proheads/120-base pRNA, where the bulk of the pRNA dissociates from the proheads during electrophoresis; 2) the prohead/120-base pRNA/gp16 complex, revealing release of pRNA/gp16 as a complex; 3) free 120-base pRNA marker.

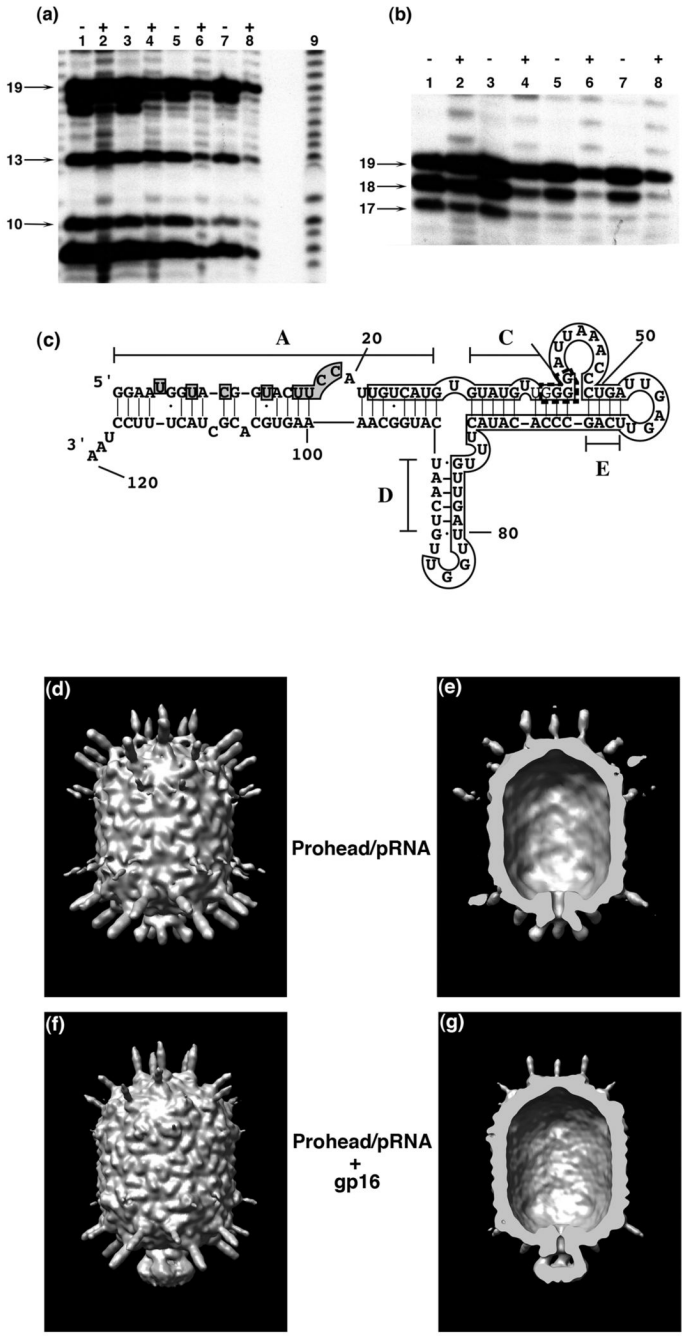

Figure 7.

Localization of gp16 on pRNA. (a)–(c) Ribonuclease footprinting of gp16 on 120-base pRNA. [^{32}P]120-base pRNA and prohead-bound [^{32}P]120-base pRNA were incubated with gp16, the mixtures treated with RNase A and the products separated by denaturing gel electrophoresis (Methods). An alkaline hydrolysis ladder was generated from 5′ end-labeled pRNA. (a) and (b) RNase A digestion. The lanes show: 1–4) treatment with 10^{-2} μg/ml RNase A; 5–8) treatment with 10^{-3} μg/ml RNase A; 1 and 5) free [^{32}P]120-base pRNA; 2 and 6) [^{32}P]120-base pRNA with gp16; 3 and 7) prohead-bound [^{32}P]120-base pRNA; and 4 and 8) prohead-bound [^{32}P]120-base pRNA with gp16. (c) gp16 and prohead composite footprint on pRNA. Shaded regions represent residues protected by gp16, the open box represents residues

protected by the prohead, and regions shown in the box bounded by the discontinuous line represent enhanced cleavages by RNase V1 when pRNA is bound to the proheads[26]. (d)–(g) Cryo-EM 3D reconstruction of the prohead/174-base pRNA/gp16 packaging intermediate. (d) prohead with 174 base pRNA. (e) Cross section of the prohead/pRNA, same view as in (d). (f) Prohead/174-base pRNA/gp16. (g) Cross section of the prohead/pRNA/gp16, same view as in (f).

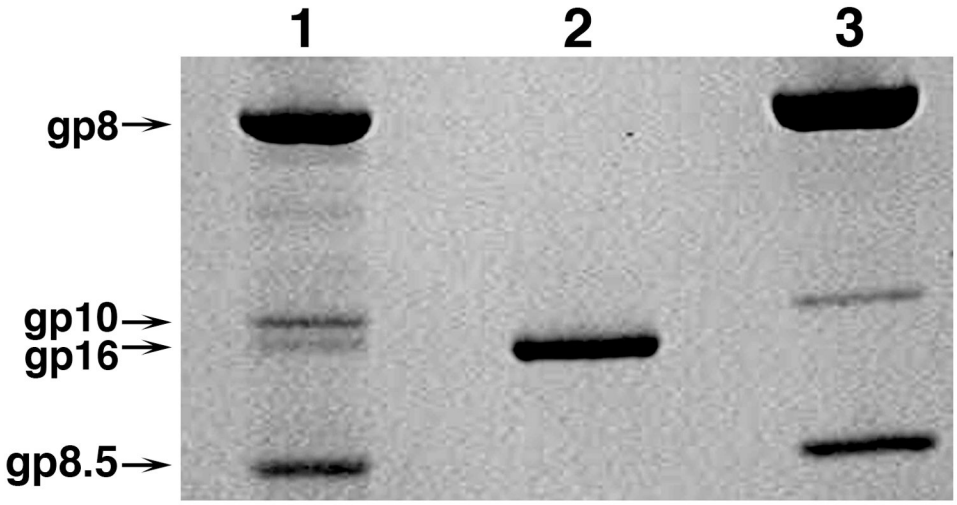

Figure 8.

The isolated DNA filled head retains gp16. SDS-PAGE analysis of DNA-filled heads isolated in a sucrose density gradient. The gradient sample was prepared by incubating proheads/pRNA for 10 min with a head-defective extract of cells from a restrictive infection with the ϕ29 mutant *sus*7(614)-*sus*8(769)-*sus*14(1241), which served as a source of DNA-gp3 and excess gp16. The lanes show: 1) filled heads consisting of capsid (gp8), connector (gp10), gp16 and head fibers (gp8.5); 2) gp16 marker; and 3) prohead marker.

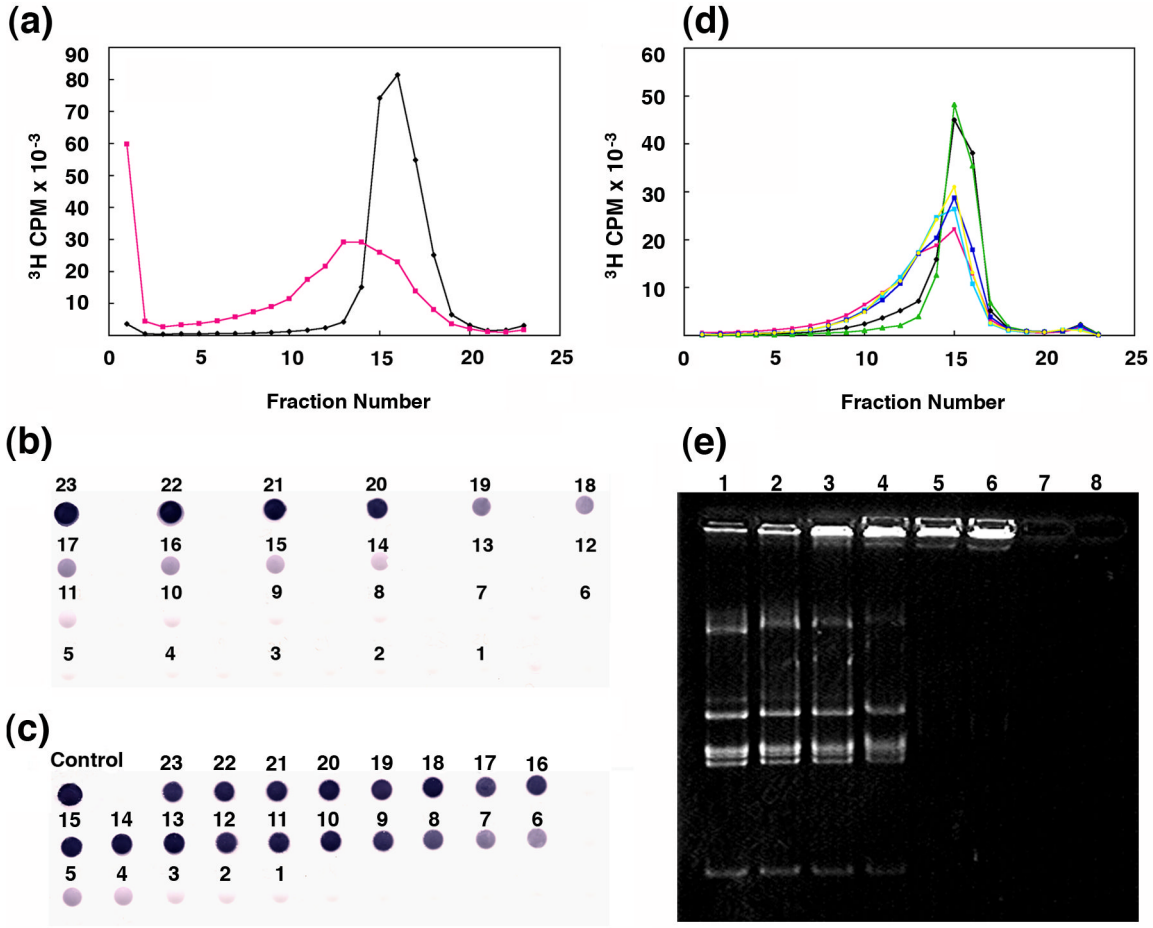

Figure 9.

Binding and supercoiling of DNA-gp3 by both gp16 and the prohead/pRNA/gp16 intermediate. (a) The sedimentation rate of DNA-gp3 was increased by binding of gp16, previously shown to be due to gp3- and gp16-dependent supercoiling of DNA-gp3[21]. The black line represents the gradient profile of DNA-gp3 and the pink line DNA-gp3 incubated with gp16. Sedimentation is from right to left. (b) Free gp16 (gradient not shown) was found primarily in the sucrose gradient fractions 23-20 in the dot-blot developed with polyclonal gp16 antiserum. (c) Dot-blot of fractions from the sucrose gradient of DNA-gp3 incubated with gp16 (Figure 9(a)), shows co-sedimentation of gp16 with DNA-gp3, notably from fraction 16 to the bottom of the gradient. (d) gp16 on the prohead-pRNA supercoils DNA-gp3. Sucrose gradient profiles of DNA-gp3 (black line), DNA-gp3 + proheads (green line), DNA-gp3 + gp16 (pink line), DNA-gp3 + gp16 + proheads (sky blue line), DNA-gp3 + gp16 complex incubated with proheads (blue line), prohead/gp16 complex incubated with DNA-gp3 (yellow line). All proheads contained 174-base pRNA. There was no alteration in the sedimentation rate of DNA-gp3 by proheads (green line). (e) Native agarose gel stained with ethidium bromide, demonstrating EMSA analysis of ϕ29 gp3-free DNA *Hpa*I fragments (6784, 2549, 2341, 1781, 1777, 1714, 1608 and 731bp) in the presence of gp16. The lanes show: 1) 0.5 μg of *Hpa*I DNA fragments; 2–6) the same DNA incubated with 6, 12, 24, 48, 48 copies of gp16 per DNA, respectively; 7) empty lane; 8) 48 copies of gp16 alone. gp16 binds to all of the *Hpa*I fragments in a sequence independent manner.

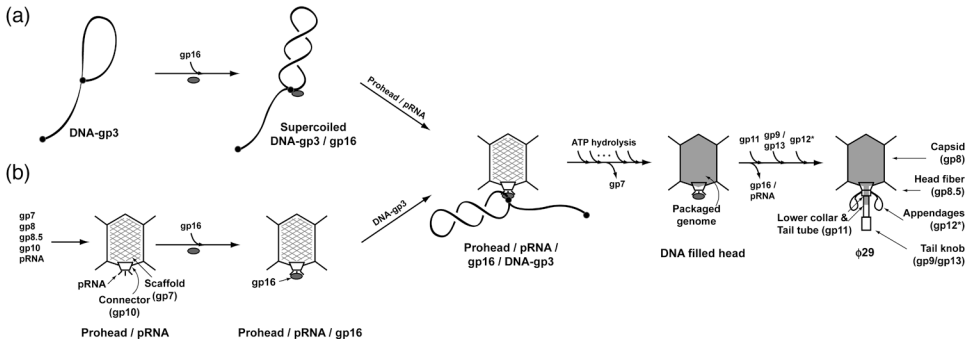

Figure 10.

Alternative pathways for producing the prohead/pRNA/gp16/DNA-gp3 packaging initiation complex. (a) DNA-gp3 forms a lariat by interaction of the terminal gp3 with DNA, independent of sequence, and gp16 binds to the lariat loop junction to effect supercoiling of the DNA in concert with gp3; this supercoiled DNA-gp3-gp16 complex is preferentially packaged[21]. (b) gp16 binds the prohead/pRNA to constitute a packaging intermediate that can be isolated and is fully active without additional gp16. This prohead/pRNA/gp16 complex is hypothesized to bind and supercoil DNA-gp3 at the prohead portal vertex. Scaffolding protein exits as packaging proceeds upon hydrolysis of ATP, and the tail components are sequentially assembled on the DNA-filled head to yield ϕ29.

Table 1

Apparent molecular mass (kDa) of gp16 by sedimentation equilibrium

gp16 (mg/ml)	5000 rpm	8000 rpm	11000 rpm
0.2	100.5	104.7	96.5
0.4	157.7	128.7	107.5
0.8	156.2	126.8	104.4

Values are calculated from the fit of 2 cells at each concentration using Nonlin[46]. Partial specific volume (υ) of 0.7375, density (σ) of 1.02859, and viscosity (η) of 0.00167 were calculated using SEDNTERP[79]. See methods for details.

Table 2

Wild-type and truncated forms of pRNA tested for gp16 binding

pRNA	Type	Prohead Binding	gp16 Binding	Packaging Activity
174-base	Wild-type	+	+	+
120-base	Wild-type	+	+	+
106-base	3′ A-helix deletion	+	+	−
71-base	A-helix deletion	+	−	−
R7	A-helix CCA deletion	+	+	−